Molina Puerto, J.; Zille, A.; Fernández Sáez, J.; Souto, A. P.; Bonastre Cano, JA.; Cases, F. (2015). Conducting fabrics of polyester coated with polypyrrole and doped with graphene oxide. Synthetic Metals. 204:110-121. doi:10.1016/j.synthmet.2015.03.014.

Conducting fabrics of polyester coated with polypyrrole and doped with graphene oxide

J. Molina[1,2], A. Zille[2], J. Fernández[1], A.P. Souto[2], J. Bonastre[1], F. Cases[1]*

[1]*Departamento de Ingeniería Textil y Papelera, EPS de Alcoy, Universitat Politècnica de València, Plaza Ferrándiz y Carbonell s/n, 03801 Alcoy, Spain*

[2]*2C2T - Centro de Ciência e Tecnologia Têxtil, Universidade do Minho, Campus de Azurém, 4800-058 Guimarães, Portugal*

Abstract

Polyester (PES) has been coated with polypyrrole (PPy) to produce conducting fabrics. Graphene oxide (GO) has been used in different concentrations (10, 20 and 30 % weight) as counter ion to neutralize the positive charges of the PPy structure. Fourier transform infrared spectroscopy with attenuated total reflection (FTIR-ATR), energy dispersive X-ray (EDX) and X-ray photoelectron spectroscopy (XPS) of the PPy/GO powders corroborated the incorporation of GO as counter ion due to the presence of O in the EDX spectrum, as well as an excess of C, arising from GO contribution. The doping level (N^+/N) decreased with the GO content. Field emission scanning electron microscopy (FESEM) showed the formation of the PPy/GO coating and the incorporation of GO in the composite. Electrochemical impedance spectroscopy (EIS) in solid state and solution, cyclic voltammetry (CV) and scanning electrochemical microscopy (SECM) were used to test the electrical properties and electroactivity of the fabrics. There was a decrease in the electrical properties and electroactivity as the GO content increased. The conductivity of the fabrics could be tuned by varying the GO content.

Keywords: polypyrrole; graphene oxide; conducting fabric; X-ray photoelectron spectroscopy (XPS); scanning electrochemical microscopy (SECM); electrochemical impedance spectroscopy (EIS).

---

* Corresponding author. Fax.: +34 966528438; telephone: +34 966528412.

E-mail addresses: jamopue@doctor.upv.es (J. Molina), azille@2c2t.uminho.pt (A. Zille), jaferse1@posgrado.upv.es (J. Fernández), souto@det.uminho.pt (A.P. Souto), joboca@txp.upv.es (J. Bonastre), fjcases@txp.upv.es (F. Cases).

1. Introduction

The production of fabrics with new properties has received particular attention during recent years. Different properties such as electrical conduction [1], flame resistance [2], self-cleaning [3], thermal regulation [4], color change [5], solar energy production [6], photonic [7], antimicrobial [8], UV protecting [9] or even catalysis [10] have been reported. Electrical conduction has attracted special attention in the development of antistatic or smart textiles [1].

There are different methods to produce conductive fabrics, such as the incorporation of conductive particles [11], electroless deposition of metals [12], reduced graphene oxide coatings [13, 14], graphene [15] or conducting polymers synthesized either chemically [16-18] or electrochemically [19, 20]. During the formation of conducting polymers, positive charges are created in their structures. These charges need to be neutralized by molecules with negative charges (counter ion). Different counter ions, either organic or inorganic have been used for this purpose [16-18]. Here, we report the use of graphene oxide as counter ion in conducting fabrics for the first time. Graphene oxide carries a

negative charge in its structure due to the presence of carboxylic acids acquiring a negative zeta potential [21]. One of the main problems of fabrics coated with conducting polymers is the migration and loss of the counter ion when the fabrics are put in solution, mainly in basic pH where deprotonation of PPy occurs [17, 18]. The immobilization of a macroscopic material (between several microns and nanometers) such as graphene oxide in a conducting polymer structure prevents its solubilization. The aim of this paper is to obtain conducting fabrics of polyester coated with PPy/GO and characterize them chemically and electrochemically.

Polyester was coated with PPy and different contents of GO (10, 20 and 30 %). The chemical characterization of the PPy-GO coated fabrics was performed by FTIR-ATR, EDX and XPS. The electrical characterization of the fabrics was performed by EIS in solid state. FESEM was used to observe the morphology of the coatings and the incorporation of GO in the PPy structure. EIS in solution, CV and SECM were used to test the electroactivity of the different fabrics. PPy/GO pellets were also obtained by compacting the powder and these were analyzed by the majority of the mentioned techniques. Samples doped with an organic (AQSA) and an inorganic counter ion ($PW_{12}O_{40}^{3-}$) were also obtained and characterized by SECM for studying the effect of the counter ion's nature.

2. Experimental

2.1. Reagents and materials

All reagents used were of analytical grade.

For the synthesis: Monolayer graphene oxide (GO) powder was acquired from Nanoinnova Technologies S.L. (Spain). Analytical grade pyrrole (Py), ferric chloride ($FeCl_3$) and anthraquinone sulfonic acid sodium salt (AQSA) were purchased from

Merck. Acetone was acquired from Prolabo. Analytical grade phosphotungstic acid ($H_3PW_{12}O_{40}$) hydrate was supplied by Fluka.

Polyester fabrics characteristics were: fabric surface density, 100 g m^{-2}; warp threads per cm, 55; weft threads per cm, 29. These are specific terms used in the field of textile industry and their meaning can be consulted in a textile glossary [22].

For the characterization: Sulphuric acid (H_2SO_4) and potassium chloride (KCl) were purchased from Merck. Hexaammineruthenium (III) chloride ($Ru(NH_3)_6Cl_3$) and iron (III) sulfate pentahydrate ($Fe_2SO_4)_3 \cdot 5H_2O$) were used as received from Acrōs Organics.

When needed, solutions were deoxygenated by bubbling nitrogen (N_2 premier X50S). Ultrapure water was obtained from an Elix 3 Millipore-Milli-Q Advantage A10 system with a resistivity near to 18.2 MΩ·cm.

2.2. Synthesis of PPy/GO on polyester fabrics

Chemical synthesis of PPy/GO on polyester textiles was carried out similarly to previous reports [18]. Size of the samples was approximately 4 cm x 6 cm. Polyester was degreased with acetone before use. Pyrrole concentration employed was 2 g L^{-1} (~0.02 M). The molar relation of the oxidant ($FeCl_3$) used was (1:2.5) (pyrrole:$FeCl_3$). Different concentrations of GO were used as counter ion (10%, 20% and 30% respect to the pyrrole mass). The solution containing pyrrole and GO (80 ml) was placed in an ultrasound bath for 30 minutes to allow the exfoliation of the GO flakes. The second stage was the adsorption of pyrrole and GO on the PES fabric during 30 minutes. After this time, the $FeCl_3$ solution (20 ml) was added in drops and the reaction elapsed over 150 minutes at room temperature with magnetic stirring. Adsorption and reaction elapsed in a precipitation beaker. The obtained conducting fabric was washed with water to remove unbound PPy/GO. The conducting fabrics were dried in a desiccator

for at least 24 h before measurements were performed. Organic (AQSA) and inorganic ($PW_{12}O_{40}^{3-}$) molecules were also used as counter ions to compare the results obtained with those of GO. Hence, PPy/AQSA and PPy/$PW_{12}O_{40}^{3-}$ were obtained and collected for measuring their electrochemical behavior by SECM.

2.3. Preparation of PPy disks

PPy/GO, PPy/AQSA and PPy/$PW_{12}O_{40}^{3-}$ powders (0.1 g) were pressed in a press (98.1 kN) to obtain discs (13 mm diameter) that were employed to carry out the different measurements.

2.4. FTIR-ATR

FTIR-ATR with horizontal mono-rebound attenuated total reflection accessory was performed with a Nicolet 6700 Spectrometer equipped with deuterated triglycine sulfate detector. An accessory with pressure control was used to equalize the pressure in the different solid samples. A prism of ZnSe was used and spectra were collected with a resolution of 4 cm^{-1}, 400 scans were averaged for each sample. GO powders were characterized to assign their different contributions. PES fabrics uncoated and coated with PPy/GO (10%, 20% and 30% GO content) were characterized. In addition, PPy/GO powders (10%, 20% and 30% GO content) were also characterized.

2.5. X-ray photoelectron spectroscopy (XPS)

XPS measurements were performed on a VG Scientific ESCALAB200 A equipment with PISCES software for data acquisition and analysis. For analysis, an achromatic Al (Ka) X-ray source operating at 15 kV (300 W) was used, and the spectrometer, calibrated with reference to Ag 3d5/2 (368.27 eV), was operated in CAE mode with 20

eV pass energy. Data acquisition was performed with a pressure lower than 10^{-6} Pa. Spectra have been charge corrected to give the adventitious C 1s spectral component (C–C, C–H) a binding energy of 285 eV. High-resolution spectra were collected using an analysis area of ≈1 mm^2. The peaks were constrained to have equal FWHM to the main peak. This process has an associated error of ±0.1 eV. Spectra were analyzed for elemental composition using CasaXPS software (version 2.3.15). Deconvolution into sub-peaks was performed by least-squares peak analysis software, XPSPEAK version 4.1, using the Gaussian/Lorenzian sum function and Shirley-type background subtraction. The best mixture of Gaussian–Lorentzian components was defined based on the instrument and resolution (pass energy) settings used as well as the natural line width of the specific core hole.

2.6. Field emission scanning electron microscopy (FESEM) and energy dispersive X-ray (EDX)

A Zeiss Ultra 55 FESEM was used to observe the morphology of the samples using an acceleration voltage of 3 kV. Energy dispersive X-ray (EDX) measurements were performed between 0 and 10 kV.

2.7. Electrical characterization by electrochemical impedance spectroscopy (EIS)

An Autolab PGSTAT302 potentiostat/galvanostat was used to perform EIS analyses. EIS measurements were performed in the 10^5-10^{-2} Hz frequency range. The amplitude of the sinusoidal voltage used was ± 10 mV. Measurements were carried out in a two-electrode arrangement, in which the sample was located between two round copper electrodes (A = 1.33 cm^2). In the second configuration, two rectangular copper electrodes (0.5 cm × 1.5 cm) separated by 1.5 cm and pressed on the fabric sample were

used. The measured area of the fabric with this configuration was a square of 1.5 cm so the measured impedance modulus (Ω) was equal to the surface resistivity (Ω/□) [19, 20].

2.8. Electrochemical impedance spectroscopy (EIS) measurements in solution

A standard three-electrode design was used to measure the EIS response of PES-PPy/GO samples in 0.1 M H_2SO_4 solutions. An asymmetrical configuration metal/sample/electrolyte was used. The sample was mounted on a stainless steel plate (used to produce the electrical connection). An Ag/AgCl (3.5 M KCl) electrode and stainless steel rod were used as reference electrode and counter electrode, respectively. The effective area used was 0.28 cm^2.

The experimental results were also fitted using a non-linear least squares fitting minimization method by ZView software (version 2.7).

2.9. Cyclic voltammetry (CV) measurements

An Autolab PGSTAT302 potentiostat/galvanostat was used to perform CV measurements in 0.1 M H_2SO_4 medium. To produce the electrical contact with the fabrics, they were located between two Ti plates. The measurements were performed in a three-electrode arrangement. A Pt wire was used as counter electrode and its preparation consisted of a flame treatment to clean its surface prior to carrying out the synthesis, according to the method developed by Clavilier [23]. The working electrode was made by cutting a strip of the conducting fabrics. Potential measurements were referred to Ag/AgCl (3.5 M KCl) reference electrode. Oxygen was removed from solution by bubbling nitrogen gas for 15 min and then an N_2 atmosphere was maintained during the measurements. The ohmic potential drop was measured and

introduced in the Autolab software (GPES). The measurements were taken between -0.2 V and 0.7 V at different scan rates (50, 5 and 1 mV s^{-1}).

2.10. Scanning electrochemical microscopy (SECM)

SECM measurements were carried out with a scanning electrochemical microscope of Sensolytics. A three-electrode configuration cell consisting of a 25 or 100-μm-diameter Pt microelectrode, a Pt wire auxiliary electrode and an Ag/AgCl (3.5 M KCl) reference electrode. Measurements were performed in $Ru(NH_3)_6^{3+}$ 0.01 M and 0.1 M KCl (supporting electrolyte). All the experiments were carried out in an inert nitrogen atmosphere. The substrates were samples (0.5 cm^2) cut from the different fabrics PES-PPy/GO (10%), PES-PPy/GO (20%), PES-PPy/GO (30%). Additional measurements were also performed on the conductive fabrics with another redox mediator (0.01 M Fe^{3+} in 0.5 M H_2SO_4 solutions). In this case the microelectrode employed was the 100-μm-diameter one.

Disks of PPy/AQSA, PPy/$PW_{12}O_{40}^{3-}$ and PPy/GO powders with different GO contents (10, 20 and 30%) were also analyzed by SECM. In this case, the microelectrode used was the 25-μm-diameter one, since the disk sample was flat and smooth.

The samples (either fabrics or powder disks) were glued to microscope slides with epoxy resin. The microelectrode operated at a potential of -0.4 V $Ru(NH_3)_6^{3+}$, or -0.1 V (Fe^{3+}) at which the oxidized form of the redox mediator (Ox) is reduced (Red) at diffusion controlled rate. Approach curves were obtained by recording the tip reduction current as the Pt microelectrode tip was moved in z direction. Approach curves give us an indication of the electroactivity of the surface. These curves were compared to the theoretical ones (positive and negative feedback models). The substrate's surface in all the measurements were at their open circuit potential (OCP).

3. Results and discussion

3.1. FTIR-ATR characterization

Fig. 1 shows the FTIR characterization of GO and PPy-GO powders with different GO contents (10, 20 and 30 %). The band around 1540 cm^{-1} was associated to the pyrrole ring stretching vibration (C=C). C-C stretching vibration can be observed at 1450 cm^{-1}. The band at 1300 cm^{-1} was attributed to C-N stretching vibration. The characteristic bands of the bending vibration of pyrrole can be observed at 775, 1037 and 1162 cm^{-1} [16, 24]. The band at 1092 cm^{-1} was attributed to the N^{+}-H in plane deformation. The band at 956 cm^{-1} was attributed to C-C out of plane deformation. The band at 890 cm^{-1} was ascribed to C_{β}-H out of plane vibration [24]. The band at 842 cm^{-1} was ascribed to C-H rocking [25]. There was little variation of the different PPy bands with the GO content.

The spectrum of GO powders is also presented as reference. The main features are: the band around 1720 cm^{-1} which was ascribed to stretching vibrations from C=O. The peak at 1613 cm^{-1} arises from C=C from unoxidized sp^2 bonds. The band at 1220 cm^{-1} was ascribed to C-OH stretching vibrations, and finally the band around 1050 cm^{-1} was attributed to C-O stretching vibrations [13]. In the PPy/GO spectra, the presence of a band around 1700 cm^{-1} is the evidence of the presence of GO. This band corresponds to C=O stretching vibrations and suffered a displacement to lower wavenumbers due to the π-π interactions and hydrogen bonding between polypyrrole rings and GO sheets [26].

Fig. 2 shows the characterization spectra of polyester fabrics, the most representative bands are: 720 cm^{-1} (out of plane benzene group), 960 cm^{-1} (C−O stretching of glycol), 1014 cm^{-1} (in-plane vibration of benzene), 1090 cm^{-1} (ester C=O stretching), 1236 cm^{-1} (ester C=O stretching) and 1714 cm^{-1} (C=O stretching of aromatic ester) [27]. When

PES fabrics were coated with the different PPy/GO coatings, the removal of the different PES bands and the appearance of the different PPy bands that were described in Fig. 1 could be observed. The presence of the band around 1700 cm^{-1} and attributed to C=O stretching vibration in GO is also worth highlighting [26]. The PPy/GO layer is thick enough to avoid the penetration of the IR radiation until the PES substrate and hence PES bands are hardly observed.

3.2. FESEM and EDX

Fig. 3 shows the characterization of the different PPy/GO coatings on PES by SEM. Fig. 3-a shows the original PES fabric. As can be seen, the surface of the fibers is quite smooth with no mentionable features. Fig. 3-b shows the PES-PPy/GO (10%) sample. It can be seen that the fibers are coated with a continuous PPy layer. In addition, the formation of PPy/GO aggregates on the surface of the fibers can also be observed. When the GO content was increased to 20% (Fig. 3-c) and 30% (Fig. 3-d), there was not a substantial modification of the morphology. However, an increase in the GO sheets content on the fibers could be easily observed. In Fig. 3-e, the surface of the fiber coated with PES-PPy/GO (30%) is magnified for better observation. In this micrograph the incorporation of GO sheets in the PPy coating can be seen. Some GO sheets are trapped in the polymer structure (the sheets have been circled for easy observation). Fig. 3-f shows the magnification of PPy/GO aggregates in a zone where they were observed on the surface of the fibers. The GO sheets can be clearly observed on the micrograph. All the sheets are coated with a continuous layer of PPy. Fig. 3-g shows the magnification of a GO sheet coated with PPy nanoparticles [28] that agglomerate and form globular morphology. Fig. 3-h shows the morphology of a GO sheet prior to performing the PPy polymerization for comparison; GO sheet shows the characteristic wrinkles [29] that

help to locate them on the surface of the fibers [13]. The wrinkles are no longer observed after PPy deposition since the PPy film is thick enough to avoid observation. More work is in progress to evaluate the rubbing and washing fastness as well as its improvement by plasma technique treatments.

An EDX analysis was performed on the surface of the PES-PPy/GO (30%) sample as example (Fig. 4-a). The most remarkable elements are C, O and N. Carbon arises from pyrrole (C_4H_5N) and graphene oxide. Nitrogen arises from pyrrole units. And the source of oxygen is mainly graphene oxide. Taking into account the atomic nitrogen content obtained (10.83%), the carbon content arising from polypyrrole was calculated (43.32%). The source for the rest of the carbon (32.03%) corresponds to graphene oxide. The O/C (32.03/10.83) ratio obtained was 0.4; which is in agreement with previous results obtained [14]. The presence of sulfur arises from the synthesis method employed to obtain graphene oxide powders which employs sulfuric acid among other strong acids and oxidants [30].

Carbon, oxygen and nitrogen distribution maps were performed to see the local distribution of these elements on the surface of the PES-PPy/GO (30%) sample (Fig. 4-b, c, d, respectively). The analyses were performed with FESEM, where no additional coating was applied on the surface of the samples. Oxygen is well distributed on the surface of the fiber, which indicates that GO has been incorporated in the PPy structure. Nitrogen arising from PPy was also well distributed on the surface of the fibers which indicates a uniform deposition of PPy.

3.3. X-ray photoelectron spectroscopy (XPS)

The relative chemical composition (C, N, O and Cl) and atomic ratios (O/C and N/C) of the polypyrrole (PPy) powders synthetized with different GO concentrations as counter

ion (10, 20 and 30 %wt) and the polyester (PES) fabric coated with the PPy/GO composite were analyzed by XPS (Table 1). In the PPy/GO powders, the presence of different concentration of GO leads to significant differences in the atomic O/C and N/C, especially for 30 %wt of GO. In the presence of 30 %wt of GO, the O/C ratio is an order of magnitude higher compared to 10 and 20 %wt. These results, in addition to the significant decrease of the N/C ratio for the 30 %wt of GO, indicate a lower polypyrrole content in this sample. The fraction of powders analyzed seem to have a higher GO content and lower PPy one. The growth of PPy takes place progressively on the surface of the fabric. Positive charges are created in the structure of the polymer and they are neutralized by the negative charges provided by GO. The growth continues till the monomer is exhausted or the polymerization process is stopped. At the same time, the excess of GO and Py (pyrrole) react in solution and produce the PPy/GO powders. In the case of the PPy powders containing the 30% GO, it seems that the quantity of GO is excessive and the quantity of PPy on the GO sheets is lower than with the other GO contents (10 and 20 %). This does not happen in the case of the fabric, where GO is progressively incorporated as the film grows to compensate the positive charges created in the structure of the polymer.

On the other hand, the coated PES fabrics show only a two-fold increase in the O/C ratio in the composite with 30 wt% of GO without significant changes in the N/C ratio. These results could indicate uniform deposition of the PES-PPy/GO composite on the fibers surface and confirm that GO has been uniformly incorporated in the PPy structure.

The C1s spectra of the PPy/GO nanocomposite powders can be deconvoluted in four peaks (Figure S1 - a, b ,c) centered at 284.6, 285.5, 287.1 and 288.5 eV attributed to the C–C, C–N, C–OH/C=O, and O-C=O, respectively [14, 31]. A fifth satellite peak at 291

eV is attributed to the C1s shake-up [32]. The C1s spectra exhibit a decrease of the carbon binding to nitrogen as function of the GO content, which is associated to the lowering of PPy in the composite (Table 2). At the same time, the increase in intensity of the peak associated with the C-C component and with the carbons binding to oxygen (especially the O-C=O) confirms the incorporation of GO in the polymer matrix [31, 33]. It was not possible to separate the contributions of C-O and C=O peaks in the C1s region that was deconvoluted in a unique peak at 287.1 eV.

The C1s envelope of the PES-PPy/GO nanocomposite can be deconvoluted in three peaks (Fig. S1 - d, e , f) centered at 285, 286.7 and 288.5 eV attributed to the C–C/C–N, C–OH, and O-C=O, respectively. A fourth satellite peak at 291 eV is attributed to the C1s shake-up [32]. No separate deconvolution was possible between the C-C and C-N component peaks and a unique peak centered at 285 eV was reported, suggesting a uniform incorporation of GO in the PPy structure on the coated PES [34]. The C-C/C-N component decreases to lower values (from 71% to 65%) as a function of the GO content, due to the lowering on the C-N component of the PPy structure.

Interestingly, the peak previously observed at 287.1 eV shifted to a lower value at 286.7 eV attributed to the presence of carbon single bonded to oxygen. However, no significant change in percentage of this component was observed in presence of different concentrations of GO. The overestimation of the C-O groups from C1s fitting could be due to the presence of the satellite component related to the electronic structure of PPy as previously observed [35]. The increase from 11% to 16% of the peak related to the O-C=O functionalities at 288.5 eV suggests that in the PPy/GO coated on the PES fibers the component of the carbons double bonded to oxygen had undergone chemical changes due to better incorporation of the two components in the nanocomposite [31].

In order to understand the different contribution of the single and double bonded oxygen in the nanocomposite synthesis, the O1s region was also analyzed. The O1s XPS spectra of PPy/GO powders are illustrated in Fig. S2 (a, b, c), which is deconvoluted into three peaks. The peaks at 530.6, 532 and 533.4 eV are ascribed to O-C=O, C=O and C–O–C/C–OH, respectively [36]. As observed before in the C1s spectra, the C-O and C=O components of the PPy/GO powders show discrepancies in the oxygen species in function of the GO content, confirming the presence of agglomerates. The increase in the carboxylic groups (from 19.4% to 39.5%) demonstrated the high level of oxidation due to the presence of increasing amount of GO in the PPy structure.

The BE values for O1s in the PES-PPy/GO (Fig. S2 – d, e, f) nanocomposite components confirm, once again, the uniform incorporation of GO in the PPy structure coated on PES. Coherence between the independent fittings of C1s and O1s signals was observed. The double bonded oxygen components can be deconvoluted in a single peak at 531.8 eV, which increases with the increase of GO in the coating, confirming the conversion of the C=O and O=C–OH groups to a new chemical species in the uniformly dispersed nanocomposite. At the same time, the peak at 533.4 eV of C-O (epoxy and alkoxy) decreases noticeably, indicating that these functional groups are partially removed [37].

In the N1s XPS core-level spectra (Fig. S3), the peak at 400.1 eV is attributed to the neutral and amine-like structure (C-N, N-H). The spectra do not show the peak at 398.3 attributed to quinonoid imine (=N–), which indicates that the PPy composites prepared present few defects [38]. Conversely, the peak at 401.7 eV is due to the positively charged nitrogen atoms with protonation ($N\text{-}H^{+}$) and is correlated with the doping level (N^{+}/N) of the composite [39]. In both the powder and PES coated PPy/GO nanocomposites, the doping level decreases with the addition of GO. The decrease of

the doping level indicates a lower conductivity of the samples. This was confirmed by electrical measurements performed by EIS.

The deconvoluted Cl2p spectra (Fig. S4) show four peaks centered at 197.5, 198.8, 200.3 and 202 eV [40, 41]. The first peak with the lowest BE corresponds to chlorine in the ionic form (Cl^- anion), while the other is indicative of intermediate chlorine species (Cl^*) due to a charge transfer between the polypyrrole backbone and the chloride [42]. This indicates a partial doping from chloride species. The two peaks located at 200.3 eV ($2p_{3/2}$) and 202 eV ($2p_{1/2}$) are attributed to covalent chloride (C-Cl) [43, 44].

3.4. Electrical characterization by EIS

EIS technique was used to measure the electrical properties of the conductive fabrics. The impedance modulus |Z| was used to measure the electrical resistance of the samples. The phase angle was used as an indication of the conductive/insulating behavior of the samples.

Fig. S5 shows the Bode plots for the samples of PES-PPy/GO (10%), PES-PPy/GO (20%) and PES-PPy/GO (30%), the averaged values of impedance modulus obtained were 0.45 Ω, 0.47 Ω and 1.09 Ω, respectively. There was an increase in the resistance of the fabrics with the increasing GO content. The –phase angle also showed values near to 0º for all the samples. A value of –phase angle of 0º indicates that the samples behave like a resistive material (conducting material). On the other hand, values of 90º would indicate a capacitive behavior (insulating material).

Sheet resistance of the fabrics was obtained with the second electrode configuration, where two rectangular copper electrodes (0.5 cm × 1.5 cm) separated by 1.5 cm and pressed on the fabric sample were used. The measured area of the fabric with this configuration was a square of 1.5 cm so the measured impedance modulus (Ω) was

equal to the surface resistivity (Ω/□) [19, 20]. The different values of surface resistivity obtained for the samples of PES-PPy/GO (10%), PES-PPy/GO (20%) and PES-PPy/GO (30%) were 177 Ω/□, 385 Ω/□, 472 Ω/□, respectively (Fig. 5). The –phase angle was also near to 0º, indicating a pure resistive behavior. There was an increase of impedance modulus and sheet resistance with the GO content. The increase of resistance with the increasing GO content is in accordance with the XPS results, where a decrease of the doping level (N^+/N) was also observed.

The fabrics obtained could be used as antistatic materials since static charging of the fibers is excluded for sheet resistance below $5 \cdot 10^9$ Ω/□ [45]. The values of surface resistivity obtained when employing an organic (AQSA) or inorganic ($PW_{12}O_{40}^{3-}$) counter ions were 45 Ω/□ and 250 Ω/□, respectively [17, 18]. The planar structure of the counter ion AQSA allows a better arrangement of PPy chains than the 3-D molecules of $PW_{12}O_{40}^{3-}$ [16]. The conductivity of the samples containing 10% GO was near to that obtained with the inorganic counter ion. Although GO is plain, its size can reach several microns (this size is the order of Å in the case of AQSA or $PW_{12}O_{40}^{3-}$). Its behavior seems to be more like a 3-D counter ion than a planar one. In bibliography, a decrease of conductivity was observed when using bulky counter ions [24]. However, bulky counter ions have the advantage that they remain retained in the polypyrrole structure due to their difficult diffusion [46].

3.5. Electrochemical impedance spectroscopy (EIS) in solution

Electrochemical impedance spectroscopy in solution was used to analyze the electrochemical behavior of the conducting fabrics. The inset in Fig. 6-b shows the equivalent electrical circuit used to fit the experimental data [47]. The equivalent electrical circuit is composed of:

- Ren: is a resistance that includes the electrolyte resistance (Re), the electronic resistance of the fabrics (Rf) and the electronic charge transfer resistance between the tweezers and the fabric (Rmfe).
- Rfsi: ionic charge transfer at the PES-PPy/GO interface corresponding to the counter ion exchange. In this case, since bulky GO acts as a negative counter ion immobilized in the PPy structure, the cations diffuse through the PPy/GO to produce the charge compensation [26].
- Cfsi: Space charge capacitance at the PES-PPy/GO corresponding to the counter ion exchange.
- Rfsie: Ion-electron charge transfer resistance at the PES-PPy/GO | solution interface with redox species.
- W: Warburg impedance due to counter-ion diffusion. W-R: Diffusion resistance. W-T: l^2/D (s), l: length of the diffusion layer, D: binary electron–ion diffusion coefficient. W-P: Warburg exponent.

Fig. 6-a show the Nyquist plots for the different conducting fabrics. In Fig. 6-b the Nyquist plot has been magnified for better observation of the high frequency region. Fig. 6-c shows the impedance modulus |Z| vs. frequency plot and Fig. 6-d represents the –phase angle vs. frequency plot. In all the plots, the experimental data has been represented by dots and the fitted data has been represented by continuous lines. The most remarkable features are the following: As can be seen in Fig. 6-b, there was a clear increase of the ionic charge transfer resistance at the PES-PPy/GO interface (Rfsi) as the GO content was increased. The other remarkable feature was the increase in the ion-electron charge transfer resistance (Rfsie) at the PES-PPy/GO textile/solution interface with redox species when the GO content was increased. The increase in Rfsie indicates a lower electroactivity of the fabrics when the GO content increased. The different

values of the fitted parameters can be observed in Table 3. Fig. 6-c shows an increase of the impedance modulus |Z| at the lower frequencies with the increasing GO content, which indicates an increase of the diffusion electrical resistance when the GO content was increased. Fig. 6-d shows the Bode plot, where two time constants can be observed. The process at high frequencies (>10^2 Hz) is due to the space charge capacitance at the PES-PPy/GO corresponding to the counter ion exchange. The process at low frequencies (10^{-1} to 10^2 Hz) with –phase angle reaching nearly 45º at 10^{-2} Hz is due to the Warburg diffusion.

3.6. Cyclic voltammetry

Fig. 7-a shows the voltammetric characterization of the PES-PPy/GO (10%) sample at different scan rates. As can be seen, the scan rate has an influence on the electrochemical response obtained. The charge transfer proceeds through the conducting polymer chains since PES is an insulating material. Only if low scan rates are used, the oxidation/reduction of PPy can be observed properly due to the slow kinetics of oxidation/ reduction on the fabrics. Otherwise, a more resistive response is obtained as observed for higher scan rates. This type of behavior has been previously observed with this type of materials and is related to the slow electron transfer [17, 48]. Yaghoubidoust et al. obtained PPy coated fabrics which showed more capacitive behavior at higher scan rates (50 $mV \cdot s^{-1}$) although a resistive form was still obtained [49]. In this case, the authors previously deposited a GO layer on the fabrics and later synthesized the PPy layer, obtaining a bilayer coating. The GO was partially reduced and this could provide conductive pathways that accelerate the electron transfer.

Fig. 7-b shows the comparison of the voltammograms of the conducting fabrics obtained with different GO contents. The scan rate of 1 $mV \cdot s^{-1}$ was used to compare the

results. As can be seen, as the GO content increases, there is a decrease of electroactivity since lower currents and lower electrical charge are obtained. The increase in the GO content leads to a decrease in the electroactivity. This result is in accordance to the results obtained by means of XPS and EIS.

3.7. Scanning electrochemical microscopy (SECM)

The electroactivity of the different PES-PPy/GO and PPy/GO samples was tested by means of SECM with feedback mode. The reduction current when the oxidized form of the redox mediator (Ox) is reduced (Red) is measured as the microelectrode approaches the surface to be studied. The potential of the microelectrode was fixed at -0.4 V, where the oxidized form of the redox mediator ($Ru(NH_3)_6^{3+}$) is reduced ($Ru(NH_3)_6^{2+}$) on the microelectrode's surface at a diffusion controlled rate (i_∞) (Fig. S6-a). The measured current is defined as $i_\infty = 4 \cdot n \cdot F \cdot D \cdot C \cdot a$, where n is the number of electrons, F is the Faraday constant, D is the diffusion coefficient, C is the bulk concentration of the redox mediator and a is the radius of the microelectrode tip.

In approach curves, the normalized reduction current registered at the microelectrode (I) is represented vs. the normalized distance (L). The normalized current is defined as follows: $I = i/i_\infty$ where "i" is the current measured at the microelectrode tip and i_∞ is the diffusion current defined above. The normalized currents depend on RG (RG=Rg/a, where Rg is the radius of the insulating glass surrounding the Pt tip of radius "a") and the normalized distance L; where L=d/a (d is the microelectrode-substrate separation). The RG of the microelectrode used in this work was $RG \geq 20$.

Depending on the distance between the microelectrode and the substrate and the electroactivity of the substrates, different situations can happen:

- If the microelectrode is far away from the substrate, the diffusion current is measured (i_∞). The normalized current (I) is equal to 1.
- If the microelectrode approaches a non-conductive substrate, there is a hindrance to the diffusion of Ox species. The surface of the sample is not able to regenerate (oxidize) the reduced form of the redox mediator (Red), hence there is a decrease in the reduction current on the surface of the microelectrode, $i<i_\infty$. This situation is known as negative feedback [50] and is characterized by $I < 1$.
- On the other hand, if the substrate is conductive, when the microelectrode approaches the surface of the sample, there is an increase in the oxidized redox species flux (Ox). The surface potential of the sample is able to regenerate (oxidize) the redox mediator. This causes an increase in the current measured on the microelectrode, $i>i_\infty$. This case is known as positive feedback [50] and is characterized by $I > 1$.

Experimental approach curves were compared with a theoretical one for positive feedback model, according to equation 1. According to Rajendran el al. [51], Pade's approximation gives a close and simple equation with less relative error for all distances and valid for RG > 10. The approximate formula of the steady-state normalized current assuming positive feedback for finite conductive substrate together with finite insulating glass thickness is:

$$I_T{}^C = \left[\frac{1 + 1.5647/L + 1.316855/L^2 + 0.4919707/L^3}{1 + 1.1234/L + 0.626395/L^2} \right] \quad (1)$$

Fig. 8-a and Fig. 8-b show the approach curves for PPy doped with an organic counter ion (AQSA) and an inorganic counter ion ($PW_{12}O_{40}^{3-}$), respectively. More positive

values of positive feedback were achieved in the case of AQSA (in the range 2.3-2.7). This indicates that PPy doped with AQSA is slightly more electroactive than when doped with the inorganic counter ion $PW_{12}O_{40}^{3-}$ (in the range 1.7-2.4). The curve for the positive feedback model is also presented for comparison as a discontinuous line in the different graphics, and as can be seen, the experimental data adjusts to the theoretical model. A comparative of electroactivity measured by SECM of PPy depending on the nature of the counter ion had not been established in bibliography to the best of our knowledge. Fig. 8-c, d, e shows the different approach curves obtained for PPy/GO pellets doped with the different GO contents (10, 20 and 30 %), respectively. All the samples presented positive feedback indicating the electroactivity of the composites. The highest electroactivity was obtained for the sample with the lowest GO content (10 %). The values of positive feedback obtained were in the range 1.8-2.1. When the GO content was increased, there was a decrease of the electroactivity and the positive feedback values were reduced to values of 1.4-1.5. However, the electroactivity was clearly reduced when comparing the results to the organic and inorganic counter ions. The electroactivity followed this order: PPy/AQSA > PPy/$PW_{12}O_{40}^{3-}$ > PPy/GO. The size of the counter ion has a clear effect on the electroactivity of the PPy samples. The higher the size of the counter ion, the lower the electroactivity is.

Fig. 8-f shows the SECM approach curves of the PES fabrics coated with PPy/GO with the different GO contents (10, 20 and 30 %). As can be seen, there was not a substantial variation in the positive feedback values and a value around 1.3 was obtained for all the fabrics. The decrease in the value of positive feedback of the conductive fabrics when compared with the pellets could be related to the existence of gaps between the fibers of the fabrics. In the gaps, there is no conductive material and the positive feedback value decreased in comparison to the continuous and flat surface of the PPy/GO pellets. The

approach curves for PES fabrics coated with PPy/AQSA and PPy/$PW_{12}O_{40}^{3-}$ followed the same trend as the pellets. The respective approach curves for both types of fabrics can be found in bibliography [17, 18].

The redox mediator $(Ru(NH_3)_6^{3+/2+}$ is an outer sphere redox mediator and is not sensitive to surface oxides [52], thus, it is not able to detect the presence of surface oxides on the GO surface. In contrast, the redox mediator $Fe^{3+/2+}$ is sensitive to surface oxides, this is why it was also used to test the electroactivity of the PES-PPy/GO fabrics. In this case, the Pt tip was polarized at 0.1 V where Fe^{3+} is reduced to Fe^{2+} at diffusion controlled rate (Fig. S6-b). Fig. 9 shows the approach curves for the fabrics coated with PPy and different GO contents. Differences in the positive feedback degree between the different fabrics were not observed, and similar curves were obtained independently of the GO content. However, an increase in the positive feedback value was observed. In this case values of positive feedback around 1.7-1.8 were achieved. This difference of positive feedback between the $(Ru(NH_3)_6^{3+/2+}$ and the $Fe^{3+/2+}$ redox mediator (1.3 vs. 1.7-1.8) can be attributed to the presence of GO in the PPy structure since the $Fe^{3+/}Fe^{2+}$ redox mediator is sensitive to surface oxides presence.

4. Conclusions

Polypyrrole doped with graphene oxide has been synthesized on polyester fabrics by chemical oxidation. This has been the first report using GO as counter ion in the production of conductive fabrics. Polypyrrole was doped with different GO contents (10%, 20% and 30%). The most remarkable fact was that conductivity and electroactivity of PES-PPy/GO could be tuned by varying the GO content in the synthesis solutions. The different chemical characterization techniques showed the formation of the PPy/GO composite. In FTIR-ATR spectra, the different PPy bands

appeared and the PES bands almost vanished indicating a good thickness of the PPy coating on the fabrics. The presence of a band at 1700 cm^{-1} corresponding to the stretching vibration of C=O indicated the incorporation of GO as counter ion. EDX showed a good distribution of oxygen in the PPy/GO coatings which indicates a good distribution of GO in the composite. XPS measurements showed an increase in the oxygen content and in the oxidized groups as the GO content increased. A decrease in the doping level of PPy (N^+/N) with the increasing GO content was also observed. Evidence for the incorporation of GO in the PPy's structure was also obtained from FESEM. The PPy/GO powders not fixed on the fibers showed the typical planar structure of GO coated with PPy in the form of globules.

The electrical properties measured by EIS, showed the increase in resistance/ surface resistivity with the GO content. In general, a decrease in electroactivity was also observed as the GO content increased, as measured by EIS in solution and CV and SECM. For SECM measurements with the fabrics, similar values of positive feedback were obtained regarding the GO content. Another redox mediator, Fe^{3+}/Fe^{2+} which is sensitive to surface oxides, confirmed the presence of GO in all the fabrics.

An organic (AQSA) and an inorganic counter ion ($PW_{12}O_{40}^{3-}$) were also used as counter ions to obtain composites with PPy and compare the results with those obtained for PPy/GO powders. When comparing the different counter ions used, the electroactivity followed this order: PPy/AQSA > PPy/$PW_{12}O_{40}^{3-}$ > PPy/GO. The decrease of electroactivity can be attributed to the increasing size of the counter ion employed. However, bulky counter ions have the advantage that they remain retained in the polymer structure.

Acknowledgements

Authors wish to thank to the Spanish Ministerio de Ciencia e Innovación (contract CTM2011-23583) for the financial support. J. Molina is grateful to the Conselleria d'Educació, Formació i Ocupació (Generalitat Valenciana) for the Programa VALi+D Postdoctoral Fellowship. Andrea Zille (C2011-UMINHO-2C2T-01) acknowledges FCT funding from Programa Compromisso para a Ciência 2008, Portugal. XPS studies were performed at CEMUP (University of Porto, Portugal) facilities. Electron Microscopy Service of the UPV (Universitat Politècnica de València) is gratefully acknowledged for help with FESEM and EDX characterization.

References

[1] Service RF. Technology - Electronic textiles charge ahead. Science. 2003;301(5635):909-911.

[2] Horrocks AR, Kandola BK, Davies PJ, Zhang S, Padbury SA. Developments in flame retardant textiles - a review. Polymer Degradation and Stability. 2005;88(1):3-12.

[3] Yu M, Wang ZQ, Liu HZ, Xie SY, Wu JX, Jiang HQ, et al. Laundering Durability of Photocatalyzed Self-Cleaning Cotton Fabric with TiO_2 Nanoparticles Covalently Immobilized. Acs Applied Materials & Interfaces. 2013;5(9):3697-3703.

[4] Shin Y, Yoo DI, Son K. Development of thermoregulating textile materials with microencapsulated phase change materials (PCM). II. Preparation and application of PCM microcapsules. Journal of Applied Polymer Science. 2005;96(6):2005-2010.

[5] Laforgue A. Electrically controlled colour-changing textiles using the resistive heating properties of PEDOT nanofibers. Journal of Materials Chemistry. 2010;20(38):8233-8235.

[6] He RR, Day TD, Krishnamurthi M, Sparks JR, Sazio PJA, Gopalan V, et al. Silicon p-i-n Junction Fibers. Advanced Materials. 2013;25(10):1461-1467.

[7] Graham-Rowe D. Photonic fabrics take shape. Nature Photonics. 2007;1(1):6-7.

[8] Vu NK, Zille A, Oliveira FR, Carneiro N, Souto AP. Effect of Particle Size on Silver Nanoparticle Deposition onto Dielectric Barrier Discharge (DBD) Plasma Functionalized Polyamide Fabric. Plasma Processes and Polymers. 2013;10(3):285-296.

[9] Carneiro JO, Teixeira V, Nascimento JHO, Neves J, Tavares PB. Photocatalytic Activity and UV-Protection of TiO_2 Nanocoatings on Poly(lactic acid) Fibres Deposited by Pulsed Magnetron Sputtering. Journal of Nanoscience and Nanotechnology. 2011;11(10):8979-8985.

[10] Lee JW, Mayer-Gall T, Opwis K, Song CE, Gutmann JS, List B. Organotextile Catalysis. Science. 2013;341(6151):1225-1229.

[11] Li Z, Luo G, Wei F, Huang Y. Microstructure of carbon nanotubes/PET conductive composites fibers and their properties. Composites Science and Technology. 2006;66(7-8):1022-1029.

[12] Zhao X, Hirogaki K, Tabata I, Okubayashi S, Hori T. A new method of producing conductive aramid fibers using supercritical carbon dioxide. Surface & Coatings Technology. 2006;201(3-4):628-636.

[13] Molina J, Fernandez J, Ines JC, del Rio AI, Bonastre J, Cases F. Electrochemical characterization of reduced graphene oxide-coated polyester fabrics. Electrochimica Acta. 2013;93:44-52.

[14] Molina J, Fernandez J, del Rio AI, Bonastre J, Cases F. Chemical and electrochemical study of fabrics coated with reduced graphene oxide. Applied Surface Science. 2013;279:46-54.

[15] Li X, Sun PZ, Fan LL, Zhu M, Wang KL, Zhong ML, et al. Multifunctional graphene woven fabrics. Scientific Reports. 2012;2.

[16] Molina J, del Rio AL, Bonastre J, Cases F. Chemical and electrochemical polymerisation of pyrrole on polyester textiles in presence of phosphotungstic acid. European Polymer Journal. 2008;44(7):2087-2098.

[17] Molina J, Fernandez J, del Rio AI, Lapuente R, Bonastre J, Cases F. Stability of conducting polyester/polypyrrole fabrics in different pH solutions. Chemical and electrochemical characterization. Polymer Degradation and Stability. 2010;95(12):2574-2583.

[18] Molina J, Fernandez J, del Rio AI, Bonastre J, Cases F. Chemical, electrical and electrochemical characterization of hybrid organic/inorganic polypyrrole/$PW_{12}O_{40}^{3-}$ coating deposited on polyester fabrics. Applied Surface Science. 2011;257(23):10056-10064.

[19] Molina J, del Rio AL, Bonastre J, Cases F. Electrochemical polymerisation of aniline on conducting textiles of polyester covered with polypyrrole/AQSA. European Polymer Journal. 2009;45(4):1302-1315.

[20] Molina J, del Rio AI, Bonastre J, Cases F. Influence of the scan rate on the morphology of polyaniline grown on conducting fabrics. Centipede-like morphology. Synthetic Metals. 2010;160(1-2):99-107.

[21] Li D, Muller MB, Gilje S, Kaner RB, Wallace GG. Processable aqueous dispersions of graphene nanosheets. Nature Nanotechnology. 2008;3(2):101-105.

[22] Complete textile glossary, available from:

http://www.composites.ugent.be/home_made_composites/documentation/Illustrated_dictionary_of_fiber_and_textile_technology.pdf, 2001. Last accessed 26th February 2015.

[23] Clavilier J. The role of anion on the electrochemical behaviour of a {111} platinum surface; an unusual splitting of the voltammogram in the hydrogen region. Journal of Electroanalytical Chemistry and Interfacial Electrochemistry. 1979;107(1):211-216.

[24] Hakansson E, Lin T, Wang HX, Kaynak A. The effects of dye dopants on the conductivity and optical absorption properties of polypyrrole. Synthetic Metals. 2006;156(18-20):1194-1202.

[25] Schlenoff JB, Xu H. Evolution of Physical and Electrochemical Properties of Polypyrrole during Extended Oxidation. Journal of the Electrochemical Society. 1992;139(9):2397-2401.

[26] Zhu CZ, Zhai JF, Wen D, Dong SJ. Graphene oxide/polypyrrole nanocomposites: one-step electrochemical doping, coating and synergistic effect for energy storage. Journal of Materials Chemistry. 2012;22(13):6300-6306.

[27] Romero E, Molina J, del Rio AI, Bonastre J, Cases F. Synthesis of PPy/$PW_{12}O_{40}^{3-}$ organic-inorganic hybrid material on polyester yarns and subsequent weaving to obtain conductive fabrics. Textile Research Journal. 2011;81(14):1427-1437.

[28] Lim SP, Pandikumar A, Lim YS, Huang NM, Lim HN. In-situ electrochemically deposited polypyrrole nanoparticles incorporated reduced graphene oxide as an efficient counter electrode for platinum-free dye-sensitized solar cells. Scientific Reports. 2014;4.

[29] Shen X, Lin XY, Yousefi N, Jia JJ, Kim JK. Wrinkling in graphene sheets and graphene oxide papers. Carbon. 2014;66:84-92.

[30] Zhong YL, Tian Z, Simon GP, Li D. Scalable production of graphene via wet chemistry: progress and challenges. Materials Today. 2015;18(2):73-78.

[31] Bose S, Kuila T, Uddin ME, Kim NH, Lau AKT, Lee JH. In-situ synthesis and characterization of electrically conductive polypyrrole/graphene nanocomposites. Polymer. 2010;51(25):5921-5928.

[32] Lisboa P, Gilliland D, Ceccone G, Valsesia A, Rossi F. Surface functionalisation of polypyrrole films using UV light induced radical activation. Applied Surface Science. 2006;252(13):4397-4401.

[33] Lim YS, Tan YP, Lim HN, Tan WT, Mahnaz MA, Talib ZA, et al. Polypyrrole/Graphene Composite Films Synthesized via Potentiostatic Deposition. Journal of Applied Polymer Science. 2013;128(1):224-229.

[34] Cairns DB, Armes SP, Chehimi MM, Perruchot C, Delamar M. X-ray photoelectron spectroscopy characterization of submicrometer-sized polypyrrole - Polystyrene composites. Langmuir. 1999;15(23):8059-8066.

[35] Malitesta C, Losito I, Sabbatini L, Zambonin PG. New findings on polypyrrole chemical structure by XPS coupled to chemical derivatization labelling. Journal of Electron Spectroscopy and Related Phenomena. 1995;76:629-634.

[36] Yang D, Velamakanni A, Bozoklu G, Park S, Stoller M, Piner RD, et al. Chemical analysis of graphene oxide films after heat and chemical treatments by X-ray photoelectron and Micro-Raman spectroscopy. Carbon. 2009;47(1):145-152.

[37] Liu P, Huang Y, Wang L, Zhang W. Synthesis and excellent electromagnetic absorption properties of polypyrrole-reduced graphene oxide–Co_3O_4 nanocomposites. Journal of Alloys and Compounds. 2013;573:151-156.

[38] Wang J, Xu Y, Zhu J, Ren P. Electrochemical in situ polymerization of reduced graphene oxide/polypyrrole composite with high power density. Journal of Power Sources. 2012;208:138-143.

[39] Zhang D, Zhang X, Chen Y, Yu P, Wang C, Ma Y. Enhanced capacitance and rate capability of graphene/polypyrrole composite as electrode material for supercapacitors. Journal of Power Sources. 2011;196(14):5990-5996.

[40] Huang Z-D, Liang R, Zhang B, He Y-B, Kim J-K. Evolution of flexible 3D graphene oxide/carbon nanotube/polyaniline composite papers and their supercapacitive performance. Composites Science and Technology. 2013;88:126-133.

[41] Zhang S, Shao Y, Liu J, Aksay IA, Lin Y. Graphene–Polypyrrole Nanocomposite as a Highly Efficient and Low Cost Electrically Switched Ion Exchanger for Removing ClO_4^- from Wastewater. ACS Applied Materials & Interfaces. 2011;3(9):3633-3637.

[42] Saoudi B, Jammul N, Chehimi MM, Jaubert AS, Arkam C, Delamar M. XPS study of the adsorption mechanisms of DNA onto polypyrrole particles. Spectroscopy-an International Journal. 2004;18(4):519-535.

[43] Ignatova M, Voccia S, Gabriel S, Gilbert B, Cossement D, Jéro□me R, et al. Stainless Steel Grafting of Hyperbranched Polymer Brushes with an Antibacterial Activity: Synthesis, Characterization, and Properties. Langmuir. 2009;25(2):891-902.

[44] Zheng J, Liu H-T, Wu B, Di C-A, Guo Y-L, Wu T, et al. Production of Graphite Chloride and Bromide Using Microwave Sparks. Scientific Reports. 2012;2.

[45] Textor T, Mahltig B. A sol-gel based surface treatment for preparation of water repellent antistatic textiles. Applied Surface Science. 2010;256(6):1668-1674.

[46] Neoh KG, Young TT, Kang ET, Kang T. Structural and mechanical degradation of polypyrrole films due to aqueous media and heat treatment and the subsequent redoping characteristics. Journal of Applied Polymer Science. 1997;64(3):519-526.

[47] Bonastre J, Molina J, del Rio AI, Galvan JC, Cases F. Study of the electrical properties of novel hybrid organic-inorganic conducting textiles of polypyrrole-phosphotungstate-polyester using electrochemical impedance spectroscopy. Synthetic Metals. 2011;161(17-18):1958-1965.

[48] Liang GJ, Zhu LG, Xu J, Fang D, Bai ZK, Xu WL. Investigations of poly(pyrrole)-coated cotton fabrics prepared in blends of anionic and cationic surfactants as flexible electrode. Electrochimica Acta. 2013;103:9-14.

[49] Yaghoubidoust F, Wicaksono DHB, Chandren S, Nur H. Effect of graphene oxide on the structural and electrochemical behavior of polypyrrole deposited on cotton fabric. Journal of Molecular Structure. 2014;1075:486-493.

[50] Sun P, Laforge FO, Mirkin MV. Scanning electrochemical microscopy in the 21st century. Physical Chemistry Chemical Physics. 2007;9(7):802-823.

[51] Rajendran L, Ananthi SP. Analysis of positive feedback currents at the scanning electrochemical microscope. Journal of Electroanalytical Chemistry. 2004;561(1-2):113-118.

[52] McCreery RL. Advanced Carbon Electrode Materials for Molecular Electrochemistry. Chemical Reviews. 2008;108(7):2646-2687.

Figure captions

Fig. 1. FTIR-ATR spectra of GO powders, and PPy/GO powders (10, 20 and 30% GO content). Resolution 4 cm^{-1}, 400 scans.

Fig. 2. FTIR-ATR spectra of PES fabrics and PES fabrics coated with PPy/GO (10, 20 and 30% GO content). Resolution 4 cm^{-1}, 400 scans.

Fig. 3. FESEM micrographs of (a) PES (x 2 K), (b) PES-PPy/GO (10%) (x 2 K), (c) PES-PPy/GO (20%) (x 2 K), (d) (e) (f) (g) PES-PPy/GO (30%) (x2 K) (x 10 K) (x 10 K) (x 50 K), (h) GO (x 50 K).

Fig. 4. a) EDX spectra and b) C, c) O and d) N distribution element maps of the PES-PPy/GO (30%) sample.

Fig. 5. Bode plots for PES-PPy/GO (10%), PES-PPy/GO (20%) and PES-PPy/GO (30%). Measurements between two copper electrodes above the samples. Distance between electrodes 1.5 cm. Textile measured area 1.5 cm x 1.5 cm. Frequency range from 10^5 Hz to 10^{-2} Hz. a) |Z| vs. frequency plot, b) –phase angle vs. frequency plot.

Fig. 6. a), b) Nyquist plots of a PES-PPy/GO (10, 20 and 30 % sample) in 0.1 M H_2SO_4 (inset, simplified equivalent circuit for metal/ PPy-GO coated PES/ non-blocking electrolyte system. c) Impedance modulus |Z| vs. frequency plot. d) –phase angle vs. frequency plot. Exposed electrode area: 0.28 cm^2. Frequency range from 10^5 to 10^{-2} Hz. (—) Fitting of experimental data.

Fig. 7. a) Cyclic voltammograms of PES-PPy/GO (30 %) at different scan rates (50, 5 and 1 $mV \cdot s^{-1}$). b) Cyclic voltammograms of PES-PPy/GO (10 %, 20 % and 30 %) at 1 $mV \cdot s^{-1}$. Second scan for all measurements.

Fig. 8. Approaching curves for: a) PPy/AQSA; b) PPy/$PW_{12}O_{40}^{3-}$; c) PPy/GO (10%); d) PPy/GO (20%); e) PPy/GO (30%); f) PES-PPy/GO (10%), PES-PPy/GO (20%) and PES-PPy/GO (30%). The theoretical positive feedback model has been included as a discontinuous line. Obtained with a 25 μm diameter Pt tip in 0.01 M $Ru(NH_3)_6^{3+}$ and 0.1 M KCl. The tip potential was -0.4 mV (vs. Ag/AgCl, 3.5 M KCl) and the approach rate was 10 $\mu m \cdot s^{-1}$. When analyzing the conducting fabrics a 100 μm diameter Pt tip was used.

Fig. 9. Approaching curves for PES-PPy/GO (10%), PES-PPy/GO (20%) and PES-PPy/GO (30%). The theoretical positive feedback model has been included as a discontinuous line. Obtained with a 100 μm diameter Pt tip in 0.01 M Fe^{3+} and 0.5 M H_2SO_4 solution. The tip potential was -0.1 V (vs Ag/AgCl) and the approach rate was 10 $\mu m \cdot s^{-1}$.

Table captions

Table 1. Relative chemical composition (At%) and atomic ratio determined by XPS of PPy/GO powders (10, 20, 30% of GO content) and PPy/GO coated on PES fabrics (10, 20, 30% of GO content).

Table 2. Results of the deconvolution analysis of the C1s, N1s, O1s and Cl2p peaks for the PPy/GO powder (10, 20, 30% of GO content) and PPy/GO coated on PES fabrics (10, 20, 30% of GO content).

Table 3. Results of the fitting of impedance data of PES-PPy/GO (10, 20 and 30% GO) in 0.1 M H_2SO_4 solution.

Table 1

Table 1. Relative chemical composition (At%) and atomic ratio determined by XPS of PPy/GO powders (10, 20, 30% of GO content) and PPy/GO coated on PES fabrics (10, 20, 30% of GO content).

	PPy/GO powders			PPy/GO coated on PES fabrics		
	GO 10%	GO 20%	GO 30%	GO 10%	GO 20%	GO 30%
C1s	69.64	71.31	43.05	73.86	73.67	68.56
N1s	12.41	14.30	3.53	13.54	13.15	11.54
O1s	14.36	11.20	49.88	10.02	10.93	17.78
Cl2p	3.58	3.19	3.54	2.59	2.26	2.12
O/C	0.21	0.16	1.16	0.14	0.15	0.26
N/C	0.18	0.20	0.08	0.18	0.18	0.17

Table 2

Table 2. Results of the deconvolution analysis of the C1s, N1s, O1s and Cl2p peaks for the PPy/GO powder (10, 20, 30% of GO content) and PPy/GO coated on PES fabrics (10, 20, 30% of GO content).

	Relative area corresponding to different chemical bonds (%)																	
	C1s (eV)							**O1s (eV)**					**N1s (eV)**		**Cl2p (eV)**			
	284.6	**285.0**	**285.5**	**286.7**	**287.1**	**288.5**	**291.0**	**530.6**	**531.8**	**532.0**	**533.4**	**535.5**	**400.1**	**401.7**	**197.5**	**198.8**	**200.3**	**202.0**
PPy/GO 10%	43.2	-	32.3	-	12.6	9.2	2.7	19.4	-	57.4	19.8	3.3	86.6	13.4	35.5	37.2	22.4	4.8
PPy/GO 20%	46.5	-	27.8	-	14.6	8.3	2.9	29.6	-	38.8	28.1	3.4	87.3	12.7	37.1	30.8	22.8	9.3
PPy/GO 30%	54.3	-	22.8	-	12.2	10.7	-	39.5	-	50.0	9.1	1.4	90.9	9.1	-	68.1	31.9	-
PES-PPy/GO 10%	-	71.1	-	16.1	-	10.8	2.0	-	63.1	-	36.9	-	88.7	11.3	49.3	32.4	12.8	5.4
PES-PPy/GO 20%	-	68.9	-	16.8	-	11.8	2.5	-	66.6	-	33.4	-	87.3	12.7	51.3	33.6	11.2	3.9
PES-PPy/GO 30%	-	65.9	-	16.5	-	15.7	1.9	-	78.7	-	21.3	-	89.2	10.8	34.9	34.8	22.6	7.7

Table 3

Table 3. Results of the fitting of impedance data of PES-PPy/GO (10, 20 and 30% GO) in 0.1 M H_2SO_4 solution.

	Chi-Sqr	**Ren (Ω)**	**Rfsi (Ω)**	**W-R (Ω)**	**W-T (s)**	**W-P**	**Cfsi (F)**	**Rfsie (Ω)**
PES-PPy/GO (10%)	0,0038	53,63	3,963	2,651	0,15	0,41	$1{,}41 \cdot 10^{-6}$	601
PES-PPy/GO (20%)	0,0043	56,88	6,72	1402	120,50	0,77	$3{,}77 \cdot 10^{-7}$	815
PES-PPy/GO (30%)	0,0043	55,06	12,61	1973	116,00	0,81	$5{,}92 \cdot 10^{-6}$	1082

Figure 1

Click here to download high resolution image

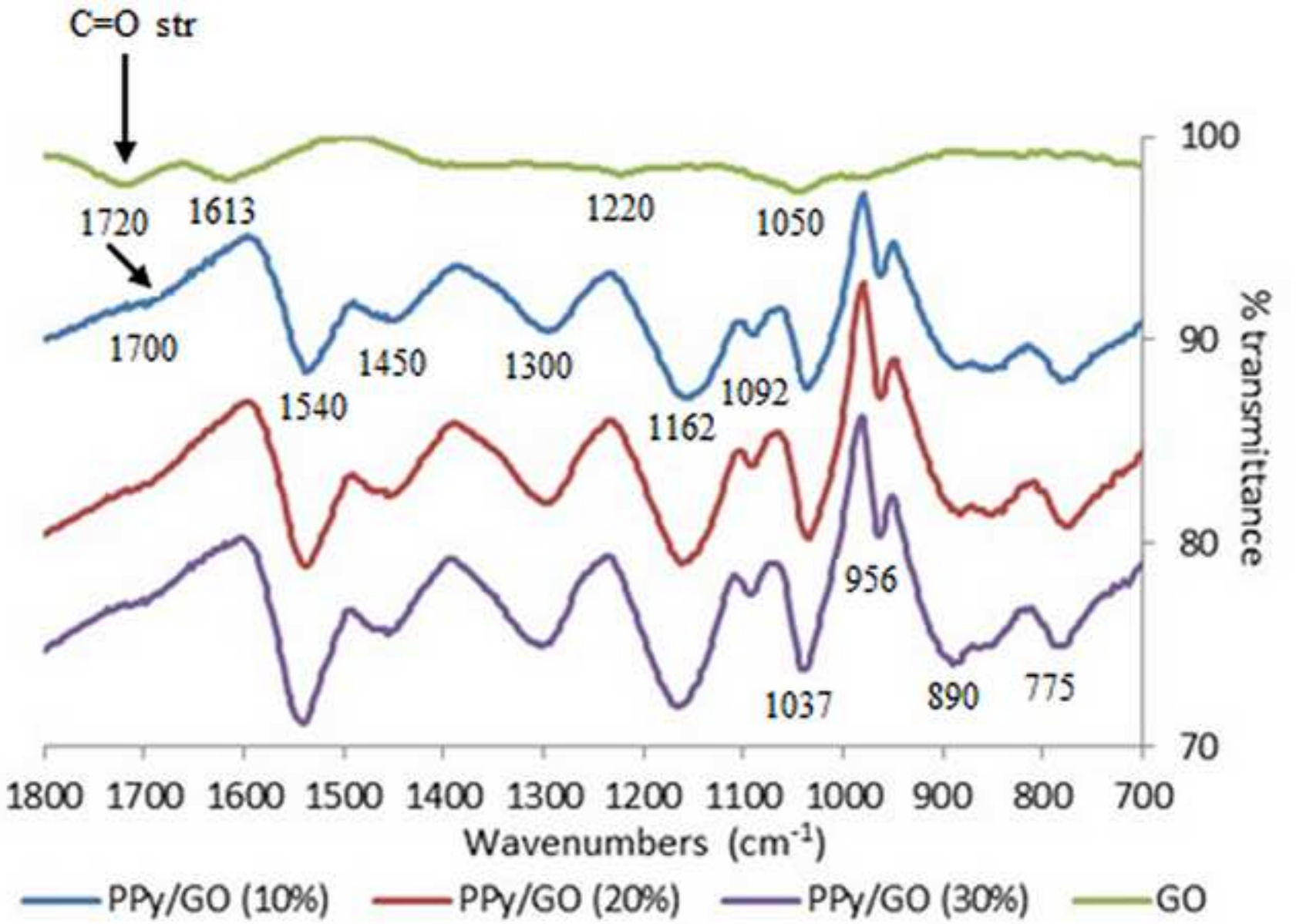

Figure 2

Click here to download high resolution image

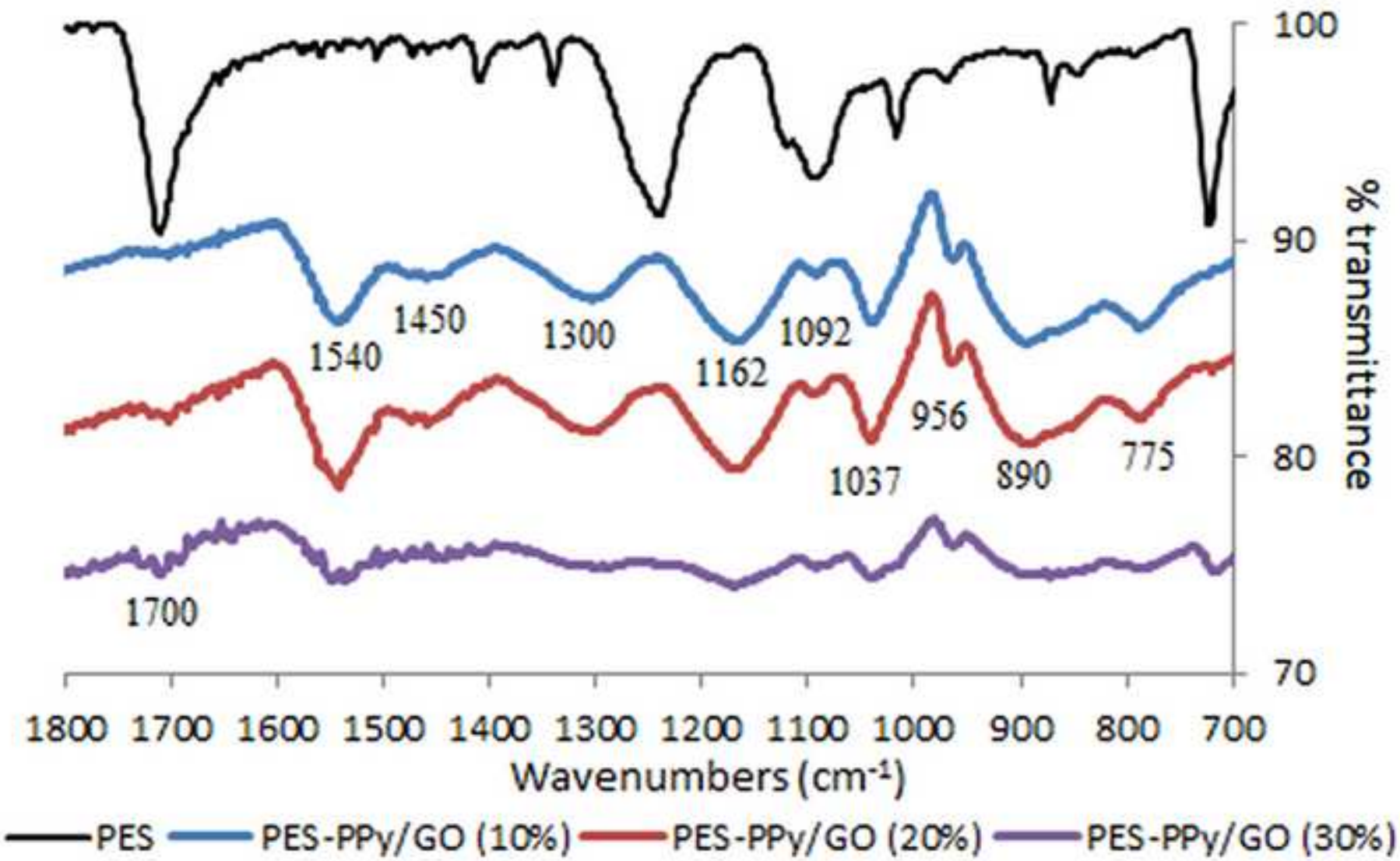

Figure 3

Click here to download high resolution image

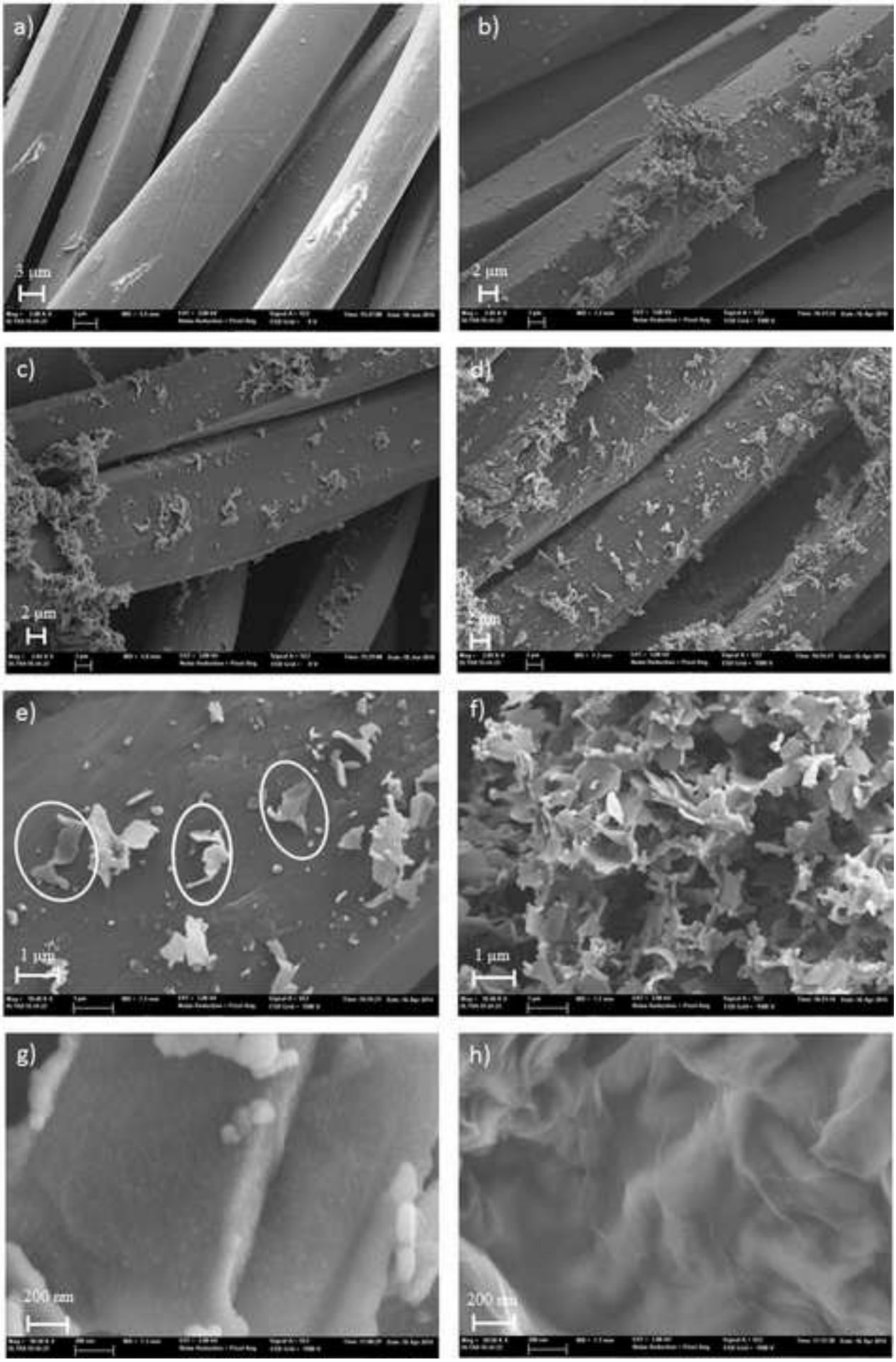

Figure 4

Click here to download high resolution image

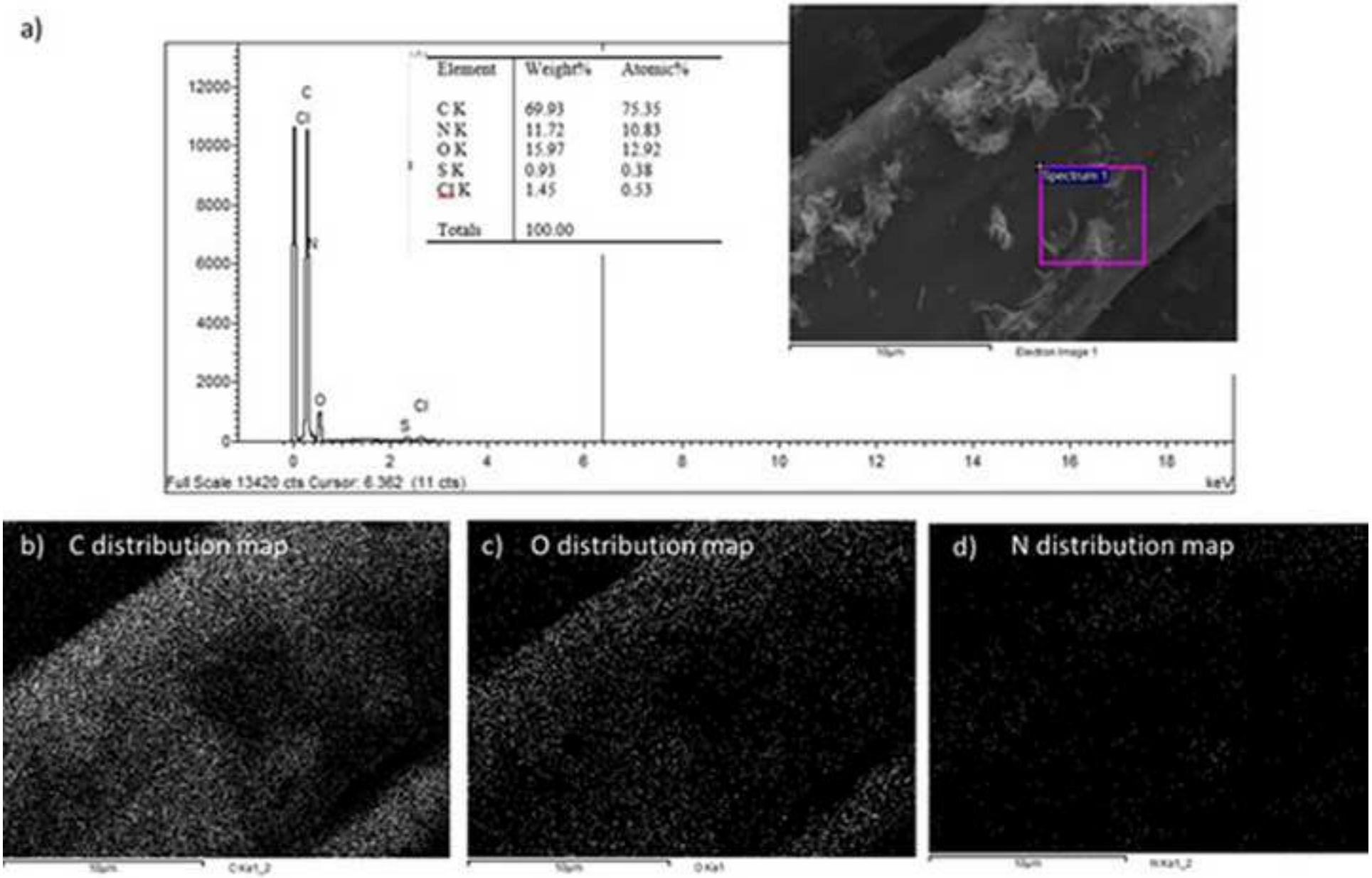

Figure 5

Click here to download high resolution image

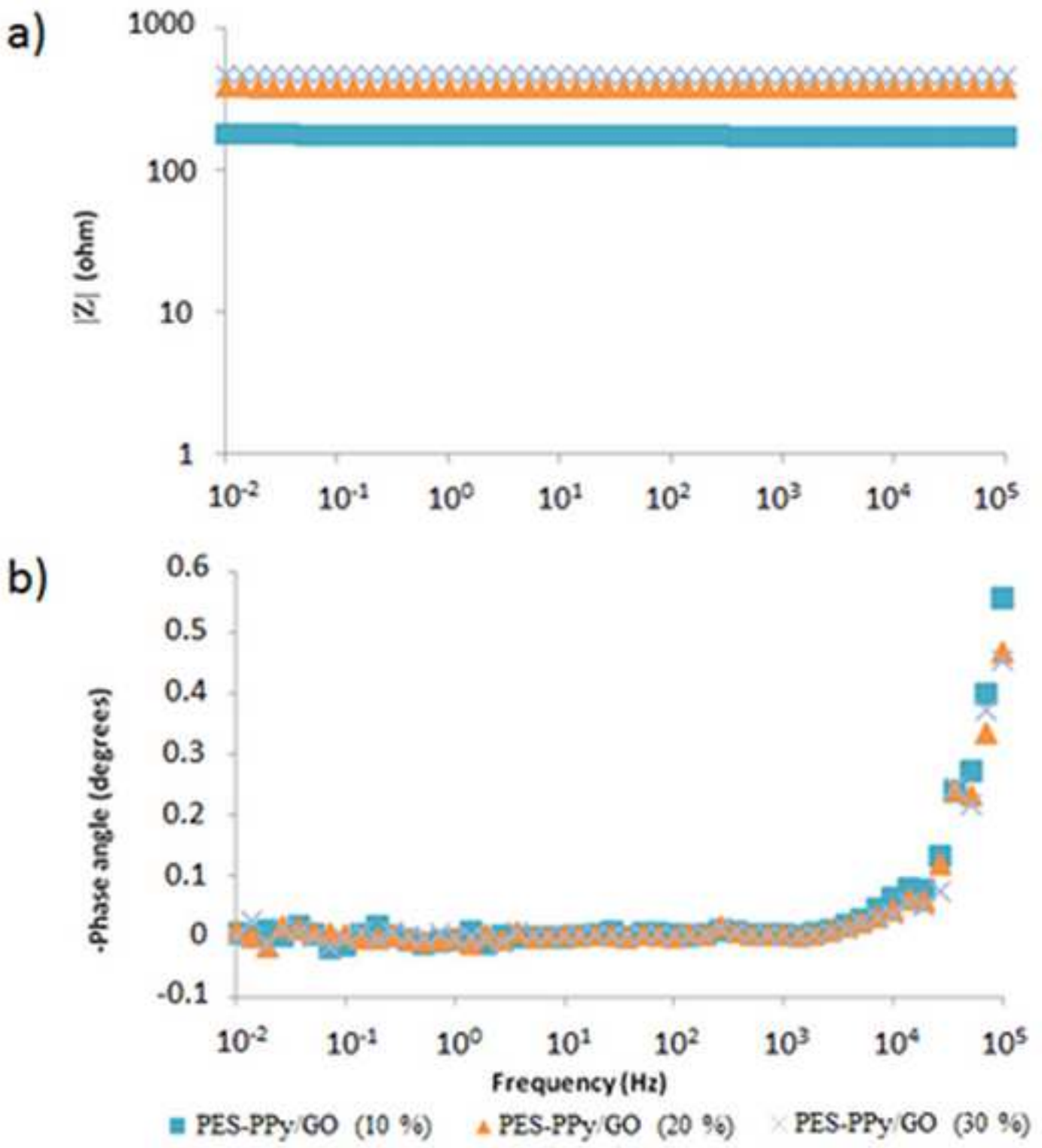

Figure 6

Click here to download high resolution image

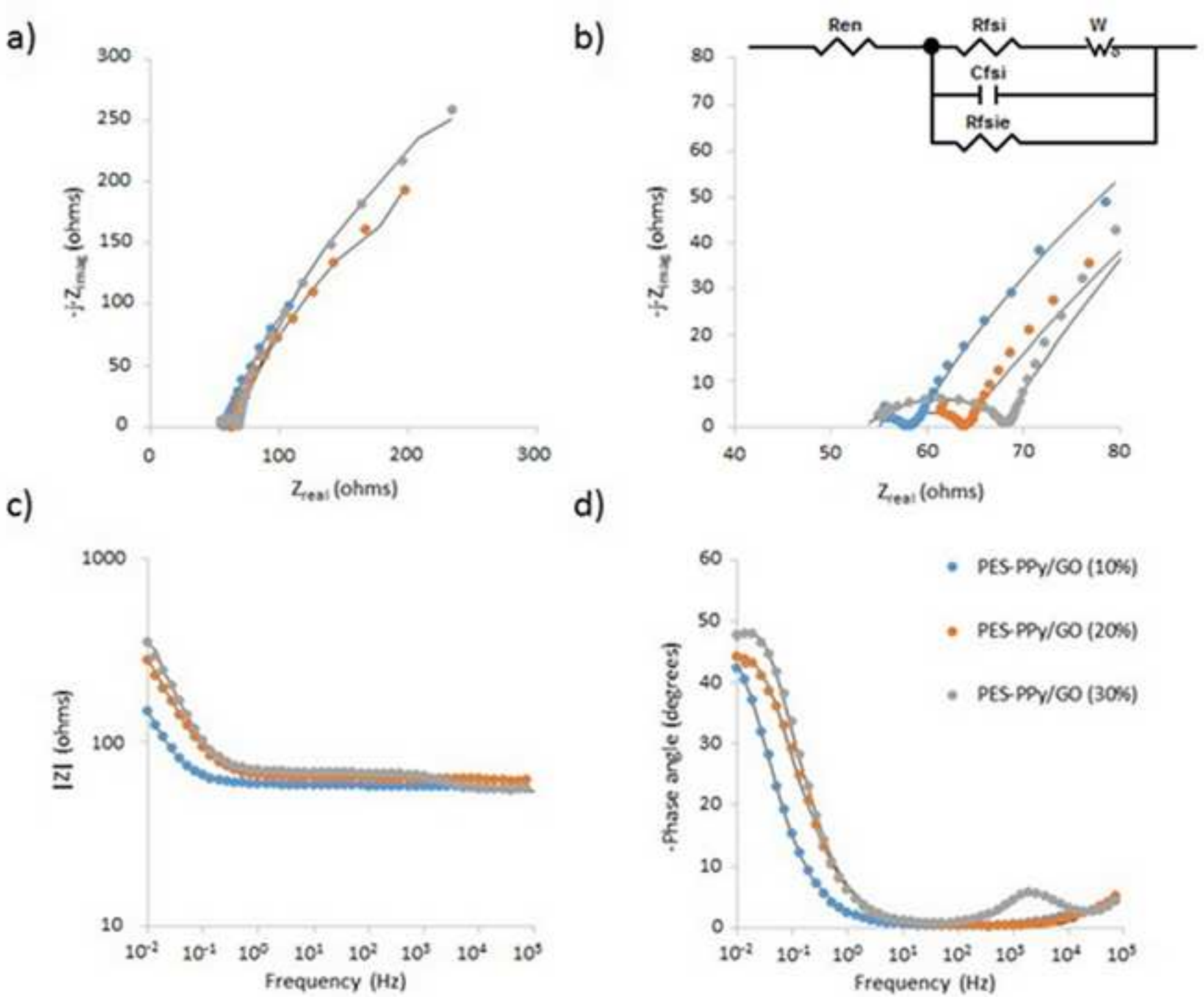

Figure 7

Click here to download high resolution image

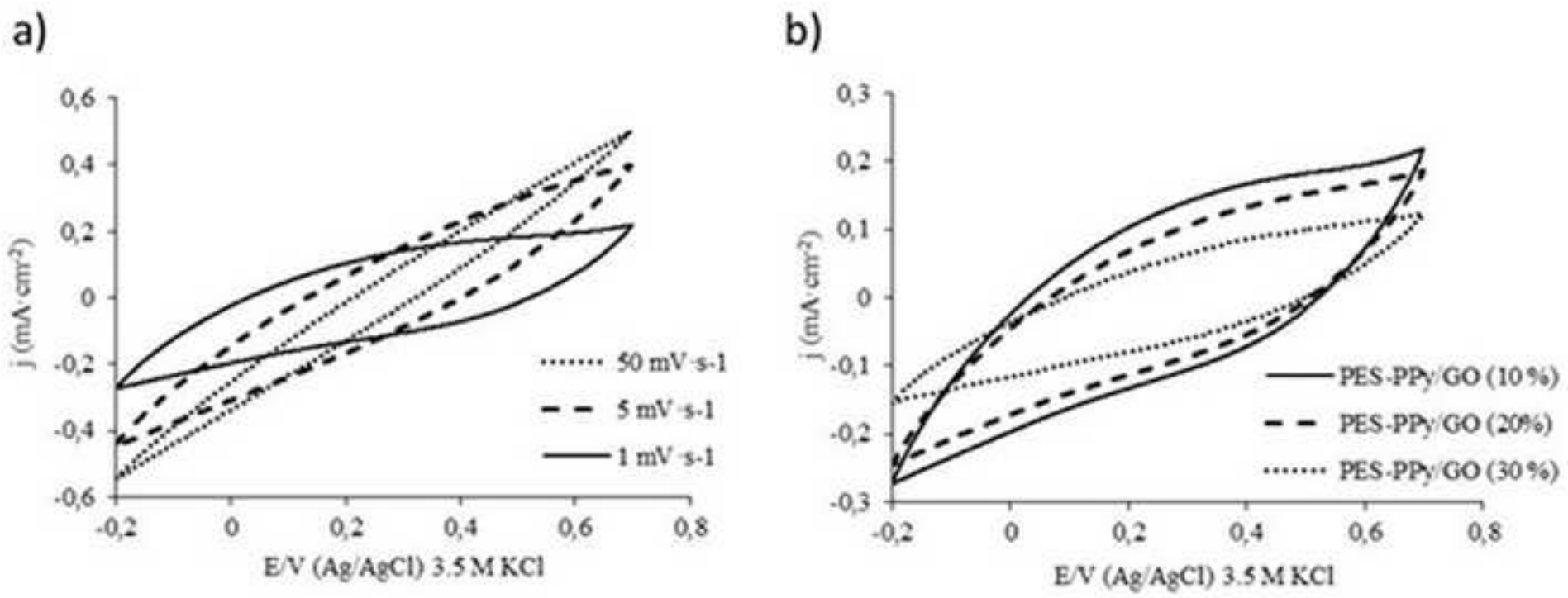

Figure 8

Click here to download high resolution image

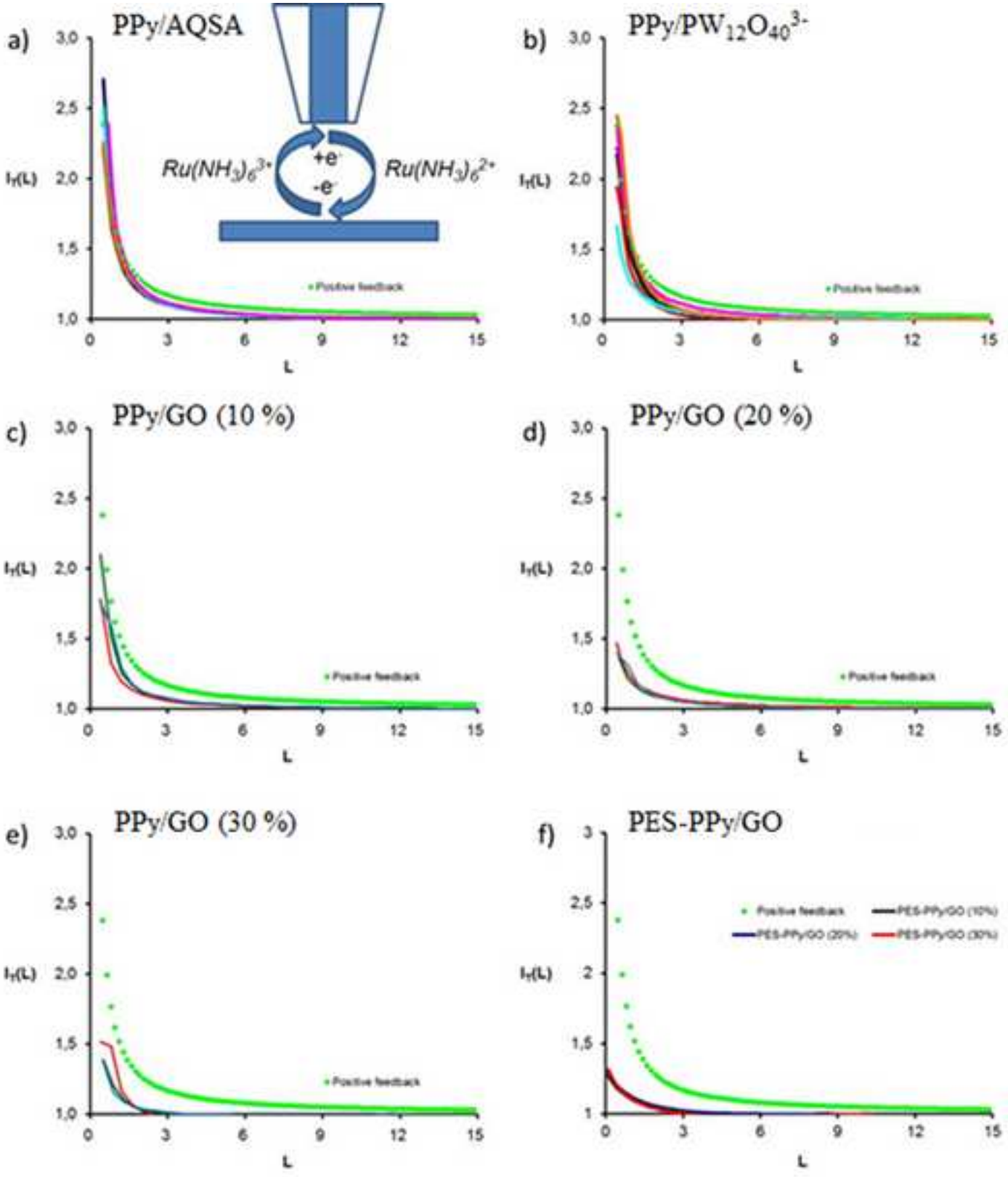

Figure 9

Click here to download high resolution image

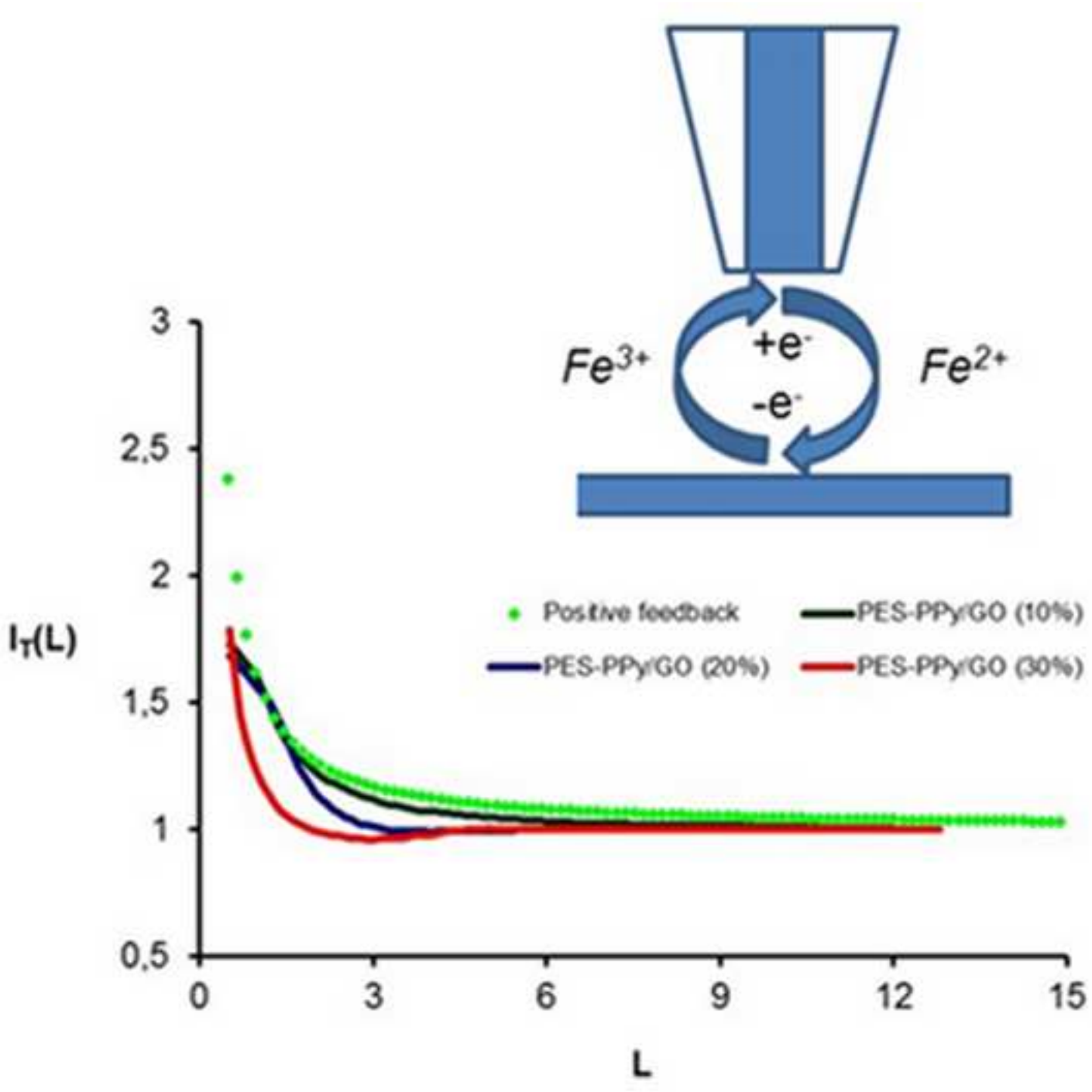

Figure S1

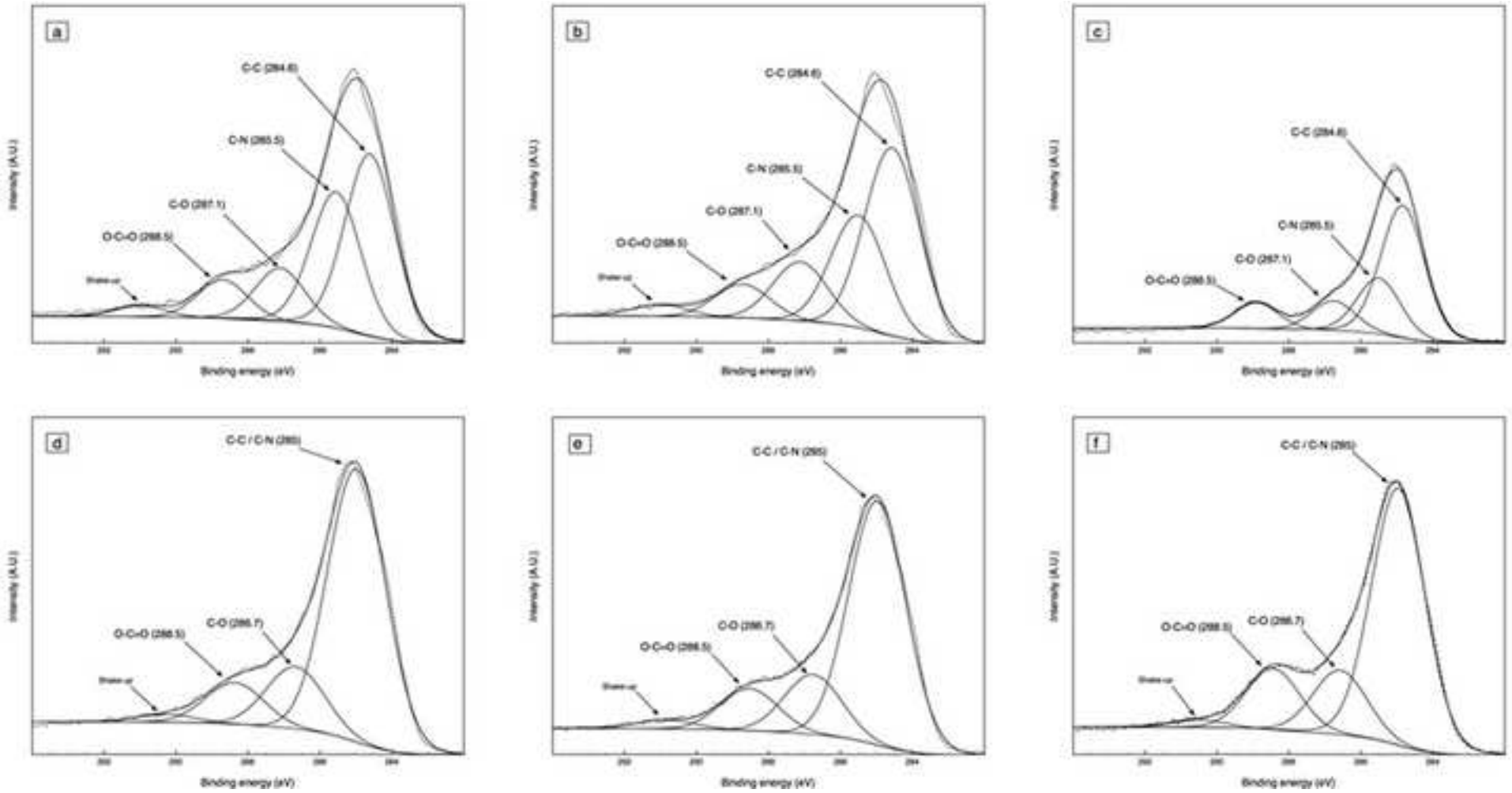
a
C-C (284.6)
C-N (285.5)
C-O (287.1)
O-C=O (288.5)
Shake-up
Intensity (A.U.)
Binding energy (eV)
b
C-C (284.6)
C-N (285.5)
C-O (287.1)
O-C=O (288.5)
Shake-up
Intensity (A.U.)
Binding energy (eV)
c
C-C (284.6)
C-N (285.5)
C-O (287.1)
O-C=O (288.5)
Intensity (A.U.)
Binding energy (eV)
d
C-C / C-N (285)
C-O (286.7)
O-C=O (288.5)
Shake-up
Intensity (A.U.)
Binding energy (eV)
e
C-C / C-N (285)
C-O (286.7)
O-C=O (288.5)
Shake-up
Intensity (A.U.)
Binding energy (eV)
f
C-C / C-N (285)
C-O (286.7)
O-C=O (288.5)
Shake-up
Intensity (A.U.)
Binding energy (eV)

Figure S2

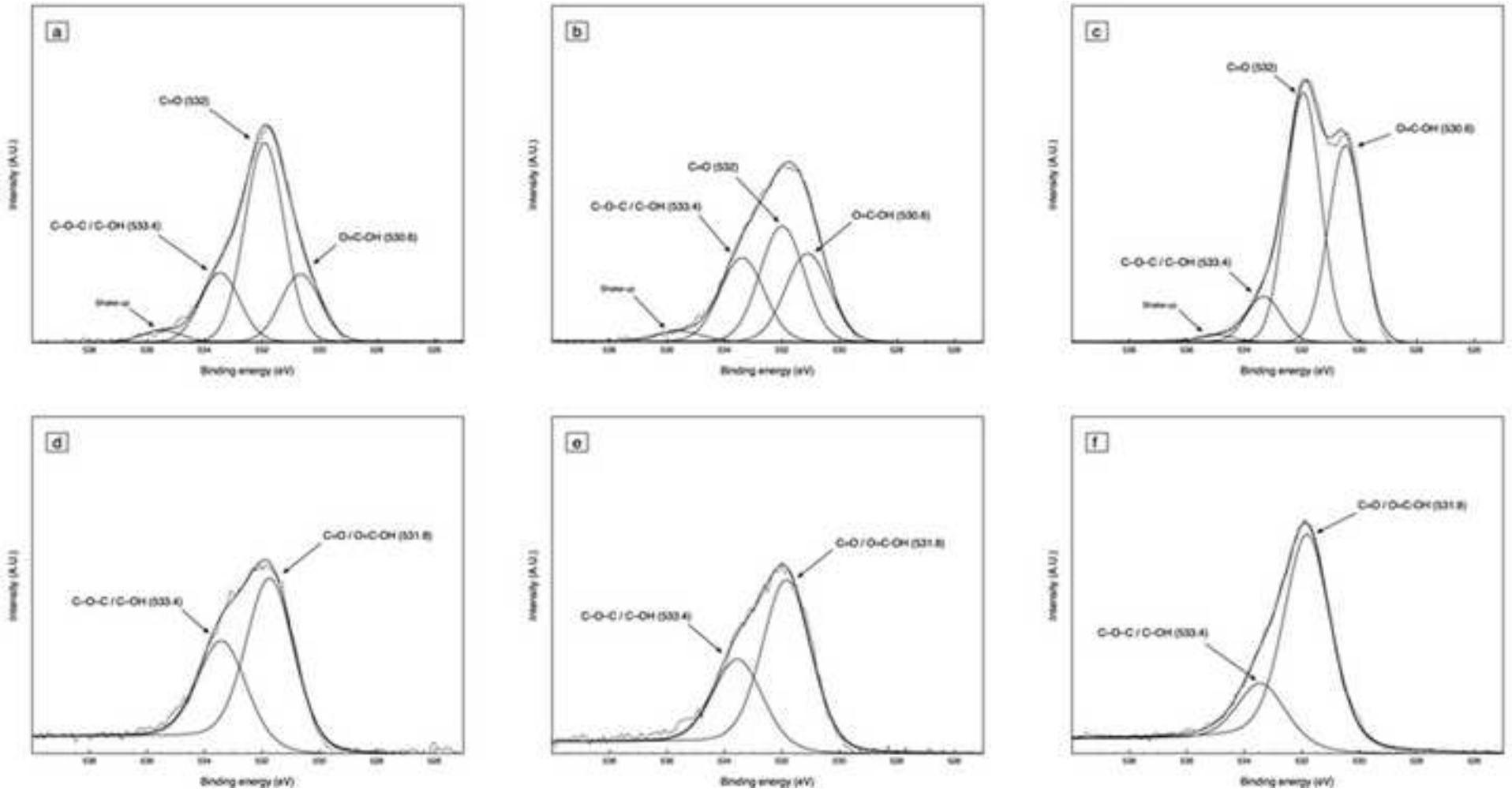
a
C=O (532)
C-O-C / C-OH (533.4)
O=C-OH (530.8)
Shake-up
Intensity (A.U.)
Binding energy (eV)
b
C=O (532)
C-O-C / C-OH (533.4)
O=C-OH (530.8)
Shake-up
Intensity (A.U.)
Binding energy (eV)
c
C=O (532)
O=C-OH (530.8)
C-O-C / C-OH (533.4)
Shake-up
Intensity (A.U.)
Binding energy (eV)
d
C=O / O=C-OH (531.8)
C-O-C / C-OH (533.4)
Intensity (A.U.)
Binding energy (eV)
e
C=O / O=C-OH (531.8)
C-O-C / C-OH (533.4)
Intensity (A.U.)
Binding energy (eV)
f
C=O / O=C-OH (531.8)
C-O-C / C-OH (533.4)
Intensity (A.U.)
Binding energy (eV)

Figure S3

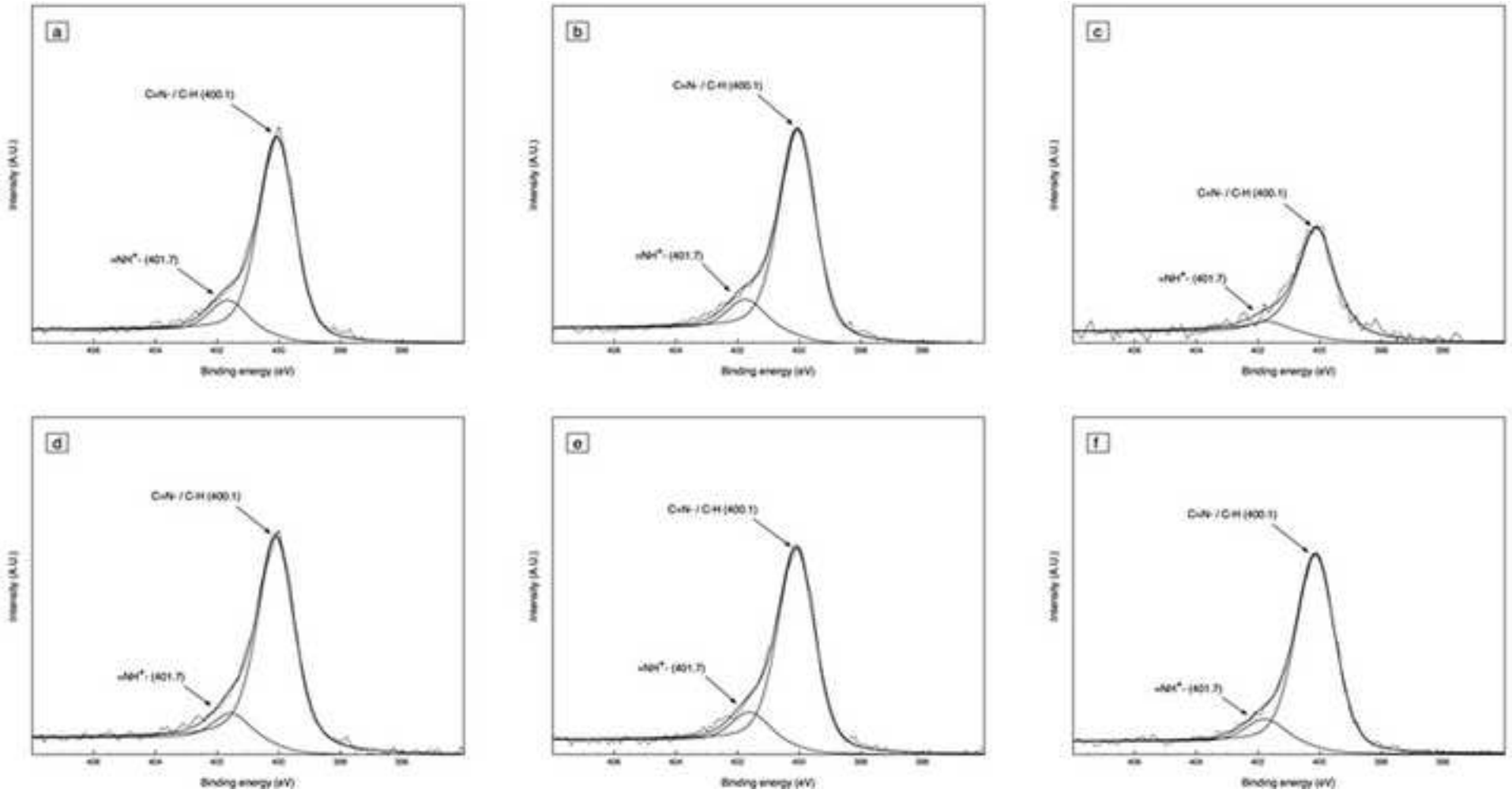
a
C=N- / C-H (400.1)
=NH+ - (401.7)
Intensity (A.U.)
Binding energy (eV)
b
C=N- / C-H (400.1)
=NH+ - (401.7)
Intensity (A.U.)
Binding energy (eV)
c
C=N- / C-H (400.1)
=NH+ - (401.7)
Intensity (A.U.)
Binding energy (eV)
d
C=N- / C-H (400.1)
=NH+ - (401.7)
Intensity (A.U.)
Binding energy (eV)
e
C=N- / C-H (400.1)
=NH+ - (401.7)
Intensity (A.U.)
Binding energy (eV)
f
C=N- / C-H (400.1)
=NH+ - (401.7)
Intensity (A.U.)
Binding energy (eV)

Figure S4

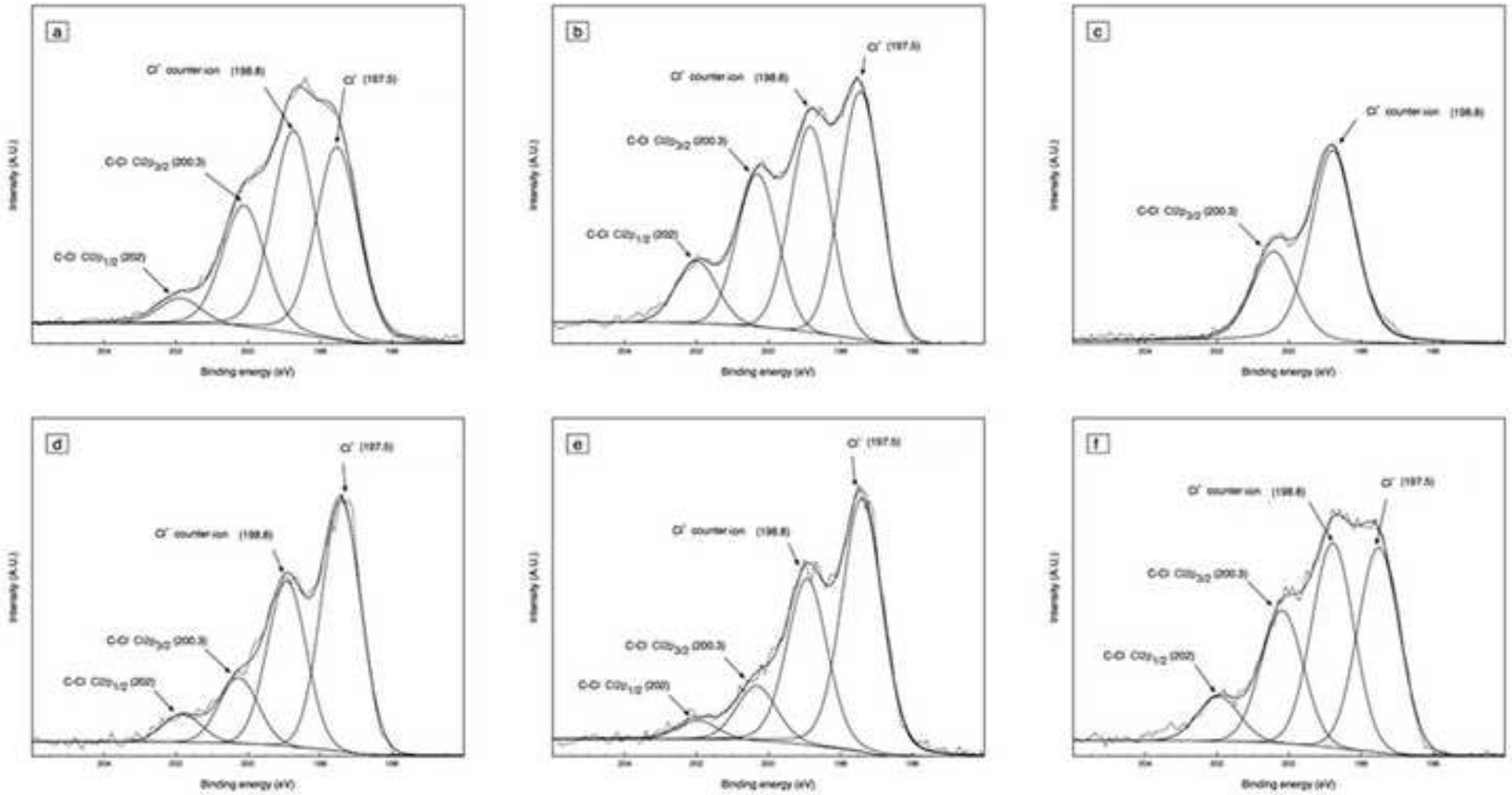
a
b
c
d
e
f
Cl⁻ counter ion (198.8)
Cl⁻ (197.5)
C-Cl Cl2p3/2 (200.3)
C-Cl Cl2p1/2 (202)
Intensity (A.U.)
Binding energy (eV)

Figure S5

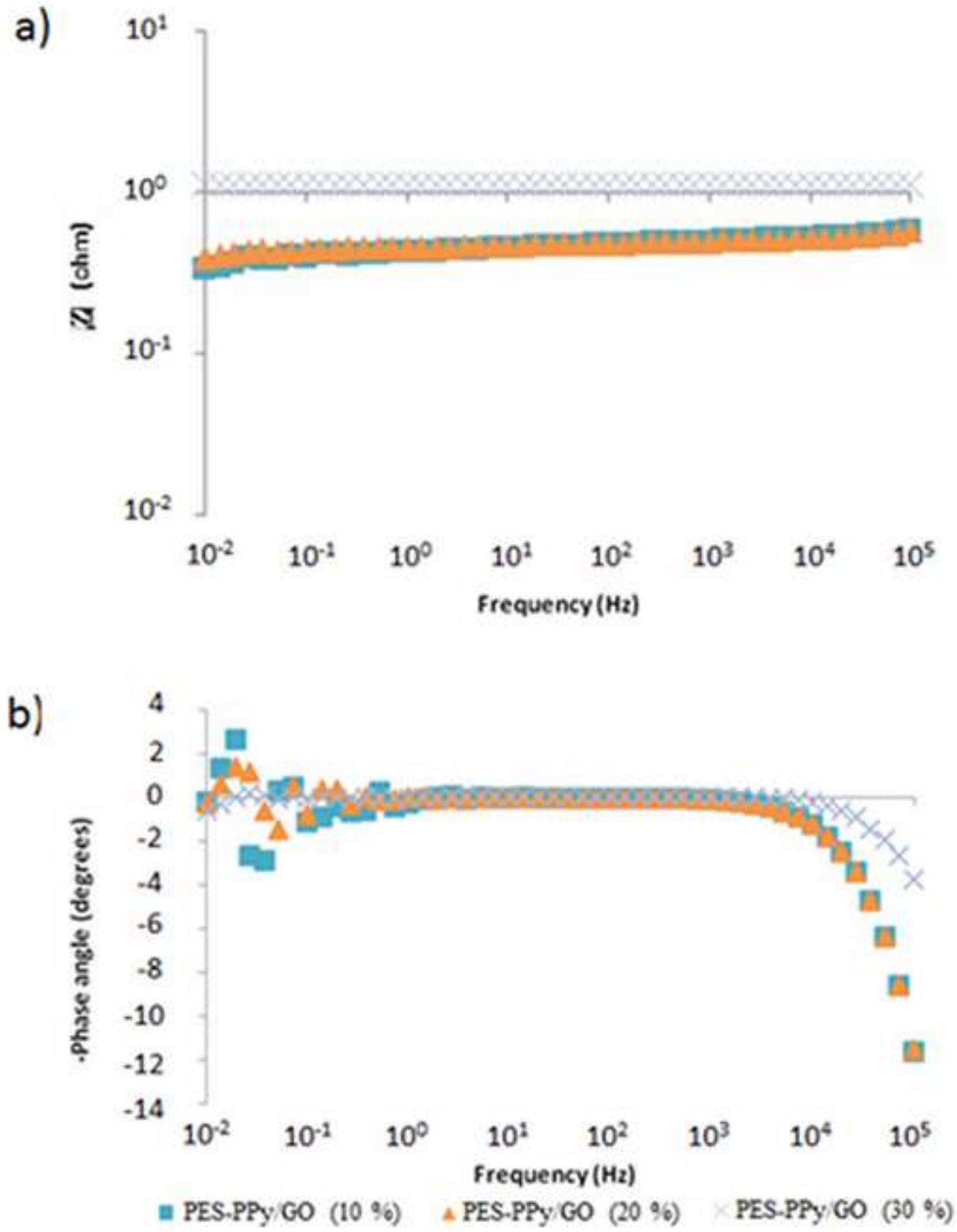
a)
10¹
10⁰
10⁻¹
10⁻²
Z (ohm)
10⁻² 10⁻¹ 10⁰ 10¹ 10² 10³ 10⁴ 10⁵
Frequency (Hz)
b)
4
2
0
-2
-4
-6
-8
-10
-12
-14
-Phase angle (degrees)
10⁻² 10⁻¹ 10⁰ 10¹ 10² 10³ 10⁴ 10⁵
Frequency (Hz)
PES-PPy/GO (10 %)
PES-PPy/GO (20 %)
PES-PPy/GO (30 %)

Figure S6

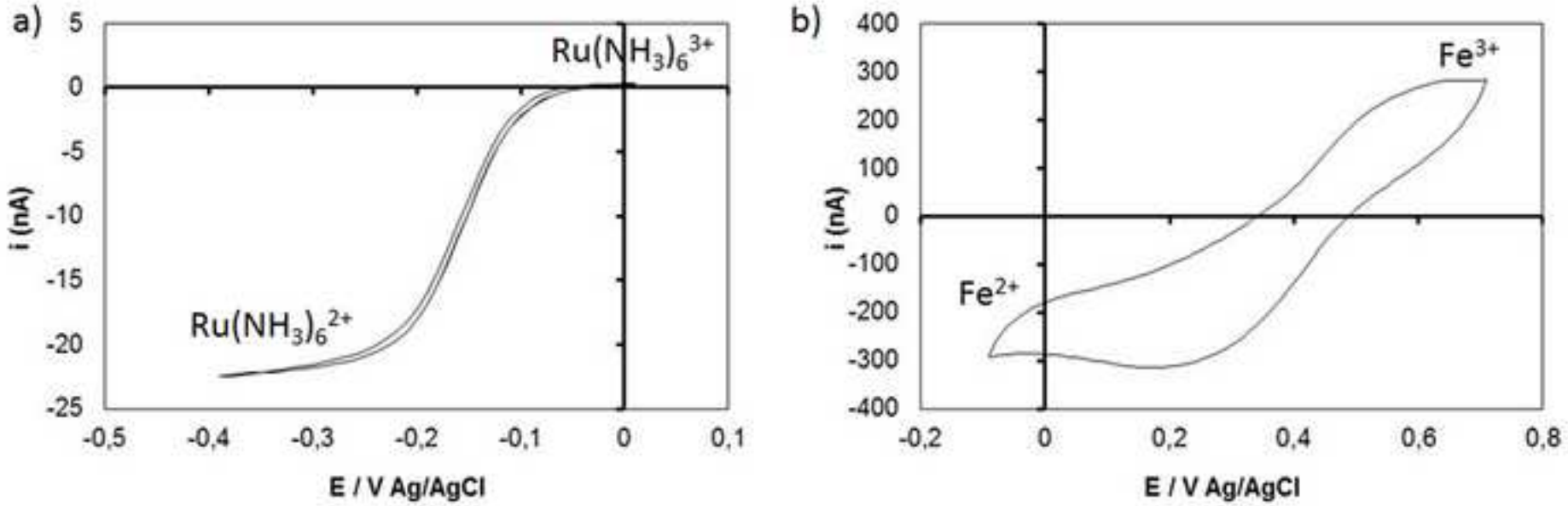
a)
5
0
-5
-10
-15
-20
-25
i (nA)
Ru(NH3)6 3+
Ru(NH3)6 2+
-0,5
-0,4
-0,3
-0,2
-0,1
0
0,1
E / V Ag/AgCl
b)
400
300
200
100
0
-100
-200
-300
-400
i (nA)
Fe3+
Fe2+
-0,2
0
0,2
0,4
0,6
0,8
E / V Ag/AgCl

Supplementary information:

Fig. S1. High-resolution deconvoluted XPS spectra with relative areas of the C1s binding energy region of PES-PPy/GO powder with 10, 20, 30% of GO content (a, b and c, respectively) and PPy/GO coated on PES fabrics with 10, 20, 30% of GO content (d, e and f, respectively).

Fig. S2. High-resolution deconvoluted XPS spectra with relative areas of the O1s binding energy region of PES-PPy/GO powder with 10, 20, 30% of GO content (a, b and c, respectively) and PPy/GO coated on PES fabrics with 10, 20, 30% of GO content (d, e and f, respectively).

Fig. S3. High-resolution deconvoluted XPS spectra with relative areas of the N1s binding energy region of PES-PPy/GO powder with 10, 20, 30% of GO content (a, b and c, respectively) and PPy/GO coated on PES fabrics with 10, 20, 30% of GO content (d, e and f, respectively).

Fig. S4. High-resolution deconvoluted XPS spectra with relative areas of the Cl2p binding energy region of PES-PPy/GO powder with 10, 20, 30% of GO content (a, b and c, respectively) and PPy/GO coated on PES fabrics with 10, 20, 30% of GO content (d, e and f, respectively).

Fig. S5. Bode plots for PES-PPy/GO (10%), PES-PPy/GO (20%) and PES-PPy/GO (30%). Sample located between two metallic conductors. Frequency range from 10^5 Hz to 10^{-2} Hz. a) |Z| vs. frequency plot, b) –phase angle vs. frequency plot.

Fig. S6. a) Cyclic voltammogram for a 25 μm diameter Pt microelectrode in 0.01 M $Ru(NH_3)_6^{3+}$ and 0.1 M KCl. The potential was scanned from +0.1 V to -0.7 V (vs. Ag/AgCl, KCl 3.5 M) at 20 $mV \cdot s^{-1}$. b) Cyclic voltammogram for the 100 μm diameter Pt microelectrode in 0.01 M Fe^{3+} and 0.5 M H_2SO_4 solution. The potential was scanned from +0.7 V to -0.1 V (vs. Ag/AgCl, KCl 3.5 M) at 20 $mV \cdot s^{-1}$.